PICK-UP REACTION FROM 100 MEV PROTONS ON LIGHT ELEMENTS.

PICK-UP REACTION FROM 100 MEV PROTONS ON LIGHT ELEMENTS

by

Jonathan Ke Ping Lee

A thesis submitted to the Faculty of Graduate Studies and Research in partial fulfilment of the requirements for the degree of Doctor of Philosophy.

J.S. Foster Radiation Laboratory
Department of Physics
McGill University
Montreal.

March 1965.

ACKNOWLEDGEMENTS

The work described in this thesis was carried out under the directorship of Dr. W.R. Frisken, who left the laboratory to take a position at Brookhaven National Laboratory in May 1964. Since then, the directorship has been assumed by Dr. R.B. Moore. To them, the author wishes to express his sincere gratitude for their guidance and assistance. Thanks are also due to Dr. R.E. Bell, Director of the laboratory, for his encouragement and assistance.

Mr. S. Doig and members of the machine shop has been very helpful in the design and development of the mechanical systems used in this work.

Throughout this work, the author has been supported by scholarships from the National Research Council of Canada. This financial assistance is gratefully acknowledged.

ABSTRACT

A particle selection system using a 14°-deflecting magnet together with a counter telescope has been designed to study (p,d) reactions from 100 Mev protons on various nuclei. The energy resolution obtained was 1.3 Mev.

The angular distributions of deuteron groups corresponding to individual levels of the residual nuclei produced in $O^{16}(p,d)O^{15}$, $C^{12}(p,d)C^{11}$ and $Li^{7}(p,d)Li^{6}$ reactions are reported. For $O^{16}(p,d)O^{15}$, two groups were observed corresponding to the ground state and 6.2 Mev state of O^{15}. From $C^{12}(p,d)C^{11}$, groups corresponding to the ground state and the 2 Mev, 4.8 Mev and 6.9 Mev states in C^{11} were observed. From $Li^{7}(p,d)Li^{6}$ groups corresponding to the ground state and the 2.2 Mev, 3.6 Mev and 5.4 Mev states in Li^{6} were observed.

Most of the angular distributions exhibited similar diffraction pattern and were believed to correspond to $\ell=1$ pick-up reactions. The dependence of the angular distribution on the total angular momentum transfer for (p,d) reactions of same orbital angular momentum transfer was observed.

TABLE OF CONTENTS

LIST OF ILLUSTRATIONS.

1. INTRODUCTION

Stripping and pick-up reactions have for some time provided a useful tool for the study of nuclear structure. As their names imply, these are reactions that involve the transfer of one or more nucleons between incident particle and the target nucleus through some form of direct interaction mechanism.

For such reactions, the energy spectra of the outgoing particles will yield information about the binding energies and pairing energies of nucleons in different shells (Cohen 1960, 1962, Goodman 1960). The angular distributions of outgoing particles corresponding to particular levels of the residual nucleus are characterized by the angular momentum ℓ of the transferred nucleon(s). Therefore the particular state of the residual nucleus can be related to the initial state of target nucleus, and in the case of single-nucleon transfer reactions, it will determine the parity and the limit of the spin of that state if the parity and spin of the target nucleus are known. Furthermore, from the magnitudes of the cross sections, the values of reduced widths for the transitions can be extracted and therefore the spectroscopic factors, which are related to the squares of the fractional parentage coefficients, can be determined. Since good energy resolution is necessary, most of the work in this field has been done at low energies ($\lesssim$ 30 Mev). Earlier works have been collected in a review article by Macfarlane and French (1960).

Most of these early results were analysed by plane wave theory (see Butler 1957), in which the distortions of the incoming and outgoing waves by the field of the target nucleus are neglected. This theory, in most cases, is capable of specifying the ℓ value for such reactions on light and intermediate elements at low energies. However, it does not match the measured angular distribution over a wide angular range. Also, it overestimates the cross section, sometimes by an order of magnitude, and therefore underestimates the reduced width, though the relative reduced width may still be useful (Macfarlane 1960). Furthermore, it does not give the correct dependence of cross section on energy of incident particles.

The distorted wave analysis (for reference, see Glenddening 1963) is a distinct improvement on the plane wave analysis, and, with the recent development of high speed electronic computers, it has become widely used. It has been successful in describing a wide variety of phenomena such as the angular distributions, cross sections and the energy dependence, which could not be described by the plane wave theory. One way of judging the reliability of such analysis is to check the consistency of the values of reduced width or spectroscopic factors deduced. At present, these values for intermediate elements seem to be consistent to within say 25% (Macfarlane 1962).

When the energy of the incident particles increases, the effects of coulomb and nuclear optical distortions decrease (Wilkinson, 1960). The larger available energy will make possible the study of such fields as the binding energies and pairing energies of nucleons of inner shells (where Q is large and negative) and the high-momentum component of the wave function of nucleons in the nucleus that are not accessible at low energy. However at higher energy, the energy spread of incident particles increases and the energy resolution becomes worse, and therefore, it is more difficult to study the individual levels of residual nuclei.

At medium energy range (say about 100 Mev - 300 Mev), present proton beams have usually an energy spread of about 1 Mev or larger, and for other particles, the energy spread is much worse (perhaps with the exception of heavy ions). Consequently, for the study of individual levels in residual nuclei, pick-up reactions can only be done in the light elements where energy level separations are large. Among these reactions, (p,d) is perhaps the easiest to handle both experimentally and theoretically.

The observation of pick-up deuterons in this energy range was first reported by Hadley and York (1950) from bombarding carbon with 90 Mev neutrons. Chew and Golberger (1950) used the plane wave Born approximation, and correlated the differential cross section with the momentum distribution of nucleons in the nucleus. Hess and Moyer (1956) bombarded various elements with 300 Mev proton and neutron beams. The production of deuterons was used to study the nuclear surface structure. Beltrametti et al (1960) used deuteron production in nuclear emulsion by 120 Mev protons to study the reaction mechanism. In all these works, the energy resolution was poor.

The study of angular distribution of deuterons corresponding to a single energy level was first done by Selove (1956) at 95 Mev. He studied $C^{12}(p,d)C^{11}$ and $Be^{9}(p,d)Be^{8}$ reactions. A prominent group corresponding to the ground state of C^{11} was observed, while for beryllium, two groups were observed -- one corresponded to the ground state and 3 Mev state and was weakly excited, and the other, corresponded to a level of 18 Mev excitation energy, and was more prominently excited. These results were compared to $He^{4}(p,d)He^{3}$ (Selove 1958) results, and the possibility of α particle structure was discussed. Cooper and Wilson (1960) studied $C^{12}(p,d)C^{11}$ by using a 145 Mev polarized proton beam.

Again, the ground state group was observed. In these reports, an energy resolution of about 3 Mev was obtained.

Recently, $C^{12}(p,d)C^{11}$ (Radvanyi 1962), $Be^{9}(p,d)Be^{8}$ (Bachelier 1962) and $O^{16}(p,d)O^{15}$ (Bachelier 1964) were reported at 155 Mev. A magnetic analyser was used, and an energy resolution of 1 Mev was obtained. This made possible the study of relatively weakly excited single levels. The angular distribution of deuterons corresponding to different levels was reported, but the angular range covered was only from 0^{o} to 30^{o}, and was insufficient to test the high-momentum component of the wave functions of neutrons in the nucleus.

In a plane wave analysis of $C^{12}(p,d)C^{11}$ at 95 Mev (Selove 1956) and 145 Mev (Cooper 1960), a high momentum component was obtained which could not be explained by independent particle model wave functions. Greider (1959), using optical distortions and the WKB approximation, was able to fit both sets of data with a one-component gaussian momentum distribution, which still showed more high-momentum component than in the independent particle model.

Benioff (1962) using the 1p-shell harmonic oscillator wave function of C^{12} together with a distortion analysis, was able to fit the results for angles smaller than 40^{o}. He suggested that the discrepancy at large angles was likely due to the forward-scattering approximation used in the analysis.

Recently, Jackson (1964) used partial wave treatment of distorted waves in her analysis of these results. The agreement was not satisfactory and she attributed the discrepancy to the approximations used and the uncertainty in the optical potential for the deuterons.

In view of these uncertainties, the present work was undertaken to study the angular distribution of deuterons corresponding to individual states of the residual nucleus. The elements studied were O^{16}, C^{12} and Li^{7}. The angular range covered was 5° to 80°. A 14°-deflecting magnet together with a dE/dx - E counter telescope was used for the detection of deuterons, and an energy resolution of 1.3 Mev was obtained.

II. PARTICLE SEPARATION METHOD.

A. General.

Since from a 100 Mev proton beam there are typically about ten times as many protons scattered from target nuclei as there are deuterons, it is imperative in a (p,d) experiment to be able to differentiate clearly between protons and deuterons. The most widely used means of differentiating are analysing magnets (Radvanyi 1962), dE/dx gating (Bennett 1959), range-energy relation (Selove 1956), dE/dx x E (Legg 1963) and time of flight (Cavanaugh 1964).

For protons, deuterons and tritons of the same energy, the loss of energy in a thin absorber such as a dE/dx scintillator will nominally have ratios of 1 : 1.7 : 2.3. In the dE/dx gating method, the pulse height from the dE/dx counter is used to separate the particles. But, dE/dx is a strong function of energy and the Landau spread of energy loss in a thin absorber tends to broaden the distribution of dE/dx output. Therefore, a narrow energy band and a reasonably thick dE/dx scintillator are necessary to obtain a good particle separation. However, protons, deuterons and tritons of the same magnetic rigidity will have energies in the ratios of 1 : 2 : 3 and dE/dx in the ratios of 1 : 2.9 : 5.7. This will then allow a considerably wider energy band to be observed.

In the present work, a magnet was designed so that the counter telescope detected only particles over a certain range of rigidity. A simple dE/dx gating was then used to separate the particles.

B. Momentum Selection With a Wedge Magnet.

For a wedge magnet with normal entrance and exit pole faces (see Fig. 1), it can be shown (Penner 1961) that

$$\begin{bmatrix} X \\ \phi \\ n \end{bmatrix} = \begin{bmatrix} 1 & L & 0 \\ 0 & 1 & 0 \\ 0 & 0 & 1 \end{bmatrix} \begin{bmatrix} \cos\theta & \rho\sin\theta & \rho(1-\cos\theta) \\ -\frac{\sin\theta}{\rho} & \cos\theta & \sin\theta \\ 0 & 0 & 1 \end{bmatrix} \begin{bmatrix} 1 & L_o & 0 \\ 0 & 1 & 0 \\ 0 & 0 & 1 \end{bmatrix} \begin{bmatrix} X_o \\ \phi_o \\ n \end{bmatrix} \qquad \text{(II-1)}$$

where X = distance of image point from central path

X_o = distance of source point from central path

L = distance from effective pole face edge (image side) to image

L_o = distance from effective pole face edge (source side) to source

ϕ_o = incident angle to magnet pole face

ϕ = exit angle to magnet pole face

θ = deflecting angle of magnet for central path

ρ = radius of curvature of central path

n = $(\rho'-\rho)/\rho$ = fractional momentum deviation from the central path.

If the second order correction of momentum deviation n is taken into account, the matrix corresponding to the magnet can be replaced by

Fig. 1. Particle trajectories in a uniform field wedge magnet with no vertical focusing. The effects of fringe fields are neglected. CC' is the central path.

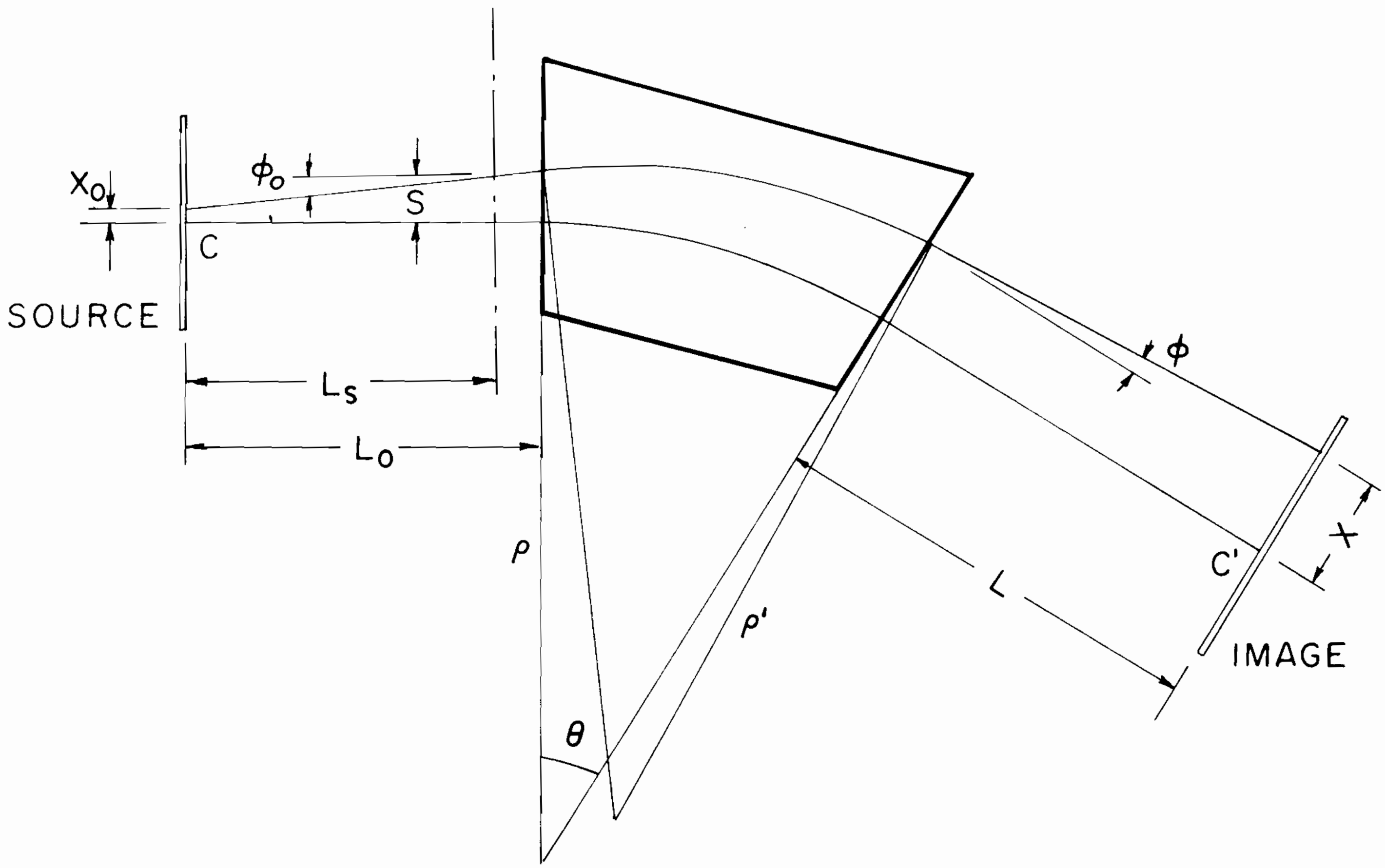

FIGURE 1

$$\begin{bmatrix} \cos\theta & \rho\sin\theta & \rho(1-\cos\theta) \\ \frac{-\sin\theta}{\rho} & \cos\theta & \frac{\sin\theta}{1-n} \\ 0 & 0 & 1 \end{bmatrix} \qquad \text{(II-2)}$$

At a plane AA' (see Fig. 1) perpendicular to the central path and in front of the entrance pole face at a distance L_s from the source, the particle from the source passes the plane at a distance S from the central path, where

$$S = X_o + \phi_o L_s \qquad \text{(II-3)}$$

If the geometry of the system is fixed, then S is a function of X_o, X and n. This expression can be derived from equations (II.1), (II.2) and (II.3) by eliminating ϕ_o and ϕ, and is represented by $S(X_o, X, n)$.

In the plane of the central path, assume that the source size extends from X_{omin} to X_{omax}, and the image size is limited from X_{min} to X_{max}, with X_{omin} and X_{min} being the points closer to the center of curvature of the central path. Defining

$$S_{max}^{(n)} = S(X_{omax}, X_{max}, n) \qquad \text{(II-4)}$$

$$S_{min}^{(n)} = S(X_{omin}, X_{min}, n)$$

particles with given n that leave the source at any point and impinge on the image at any point must pass plane AA' within $S_{min}^{(n)}$ and $S_{max}^{(n)}$. That is

$$S_{min}^{(n)} \leqslant S(X_o, X, n) \leqslant S_{max}^{(n)} \qquad \text{(II-5)}$$

if $\quad X_{omin} \leqslant X_o \leqslant X_{omax}$

and $\quad X_{min} \leqslant X \leqslant X_{max}$

Now, if a slit is placed at plane AA' with opening from S_1 to S_2 where S_1 is the point closer to the center of curvature, then

$$S_1 = S_{min}^{(n)} \quad \text{and} \quad S_2 = S_{max}^{(n)} \qquad \text{(II-6)}$$

and the values of n can be computed for each of the equations (II-6). Let these values be n_{1min} and n_{2max} respectively. In cases where n_{1min} is larger than n_{2max}, then for particles of n value between them the transmission from source to image is not affected by the slit setting. For particles of n value outside this range, the transmission efficiency gradually decreases and is equal to zero when n goes beyond a certain value. If n_{1min} is less than n_{2max}, then the transmission of all particles will be affected. This can occur when the slit setting is too narrow.

From this it can be seen that with a slit in front of a wedge magnet, the range of magnetic rigidity of particles transmitted can be controlled. The detail characteristics of such a system will be further discussed in section II-F.

C. Description of Magnet.

The magnet used was a C-frame (see Fig. 2) with

Fig. 2. Experimental Magnet. Dotted line shows the position of coils.

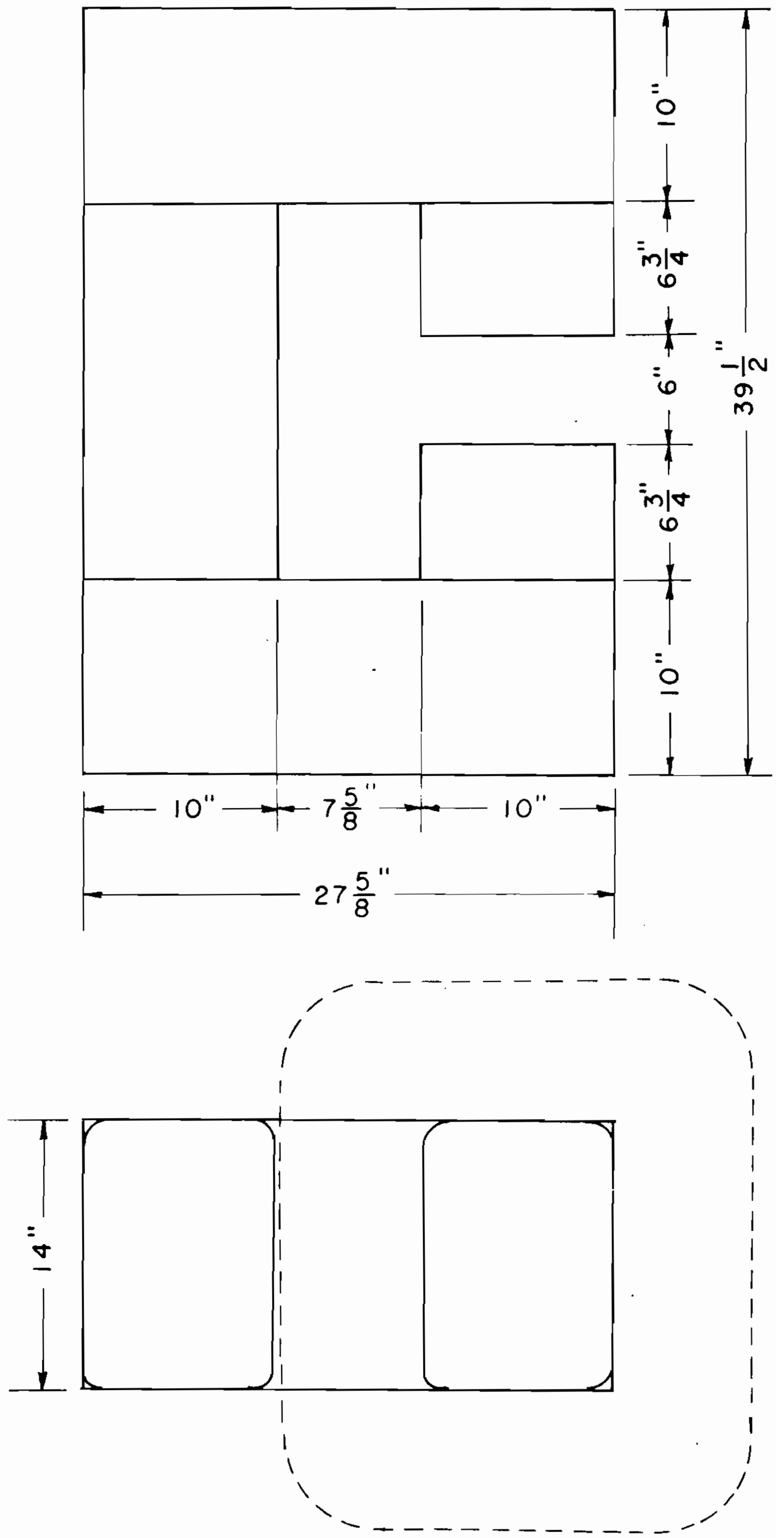

FIGURE 2

removable pole tips. The basic yoke was designed in this laboratory and built by Dominion Engineering Co. Ltd. The coils were made in this laboratory and are mechanically exchangeable with those of the switching magnet used in the beam transport system.

The pole tips used in this work were designed for a deflecting angle of 14^{o} and the pole gap was 1.16". A deflecting chamber was placed between the two pole tips. The position of the deflecting chamber and the pole tip relative to the central path is shown in Fig. 3. Spacers were used to fix the pole tip gap, and the pole tips and chamber were held together as a single unit to be inserted between the surfaces of the basic yoke. The magnetic flux at central region for different current was measured by a Hall probe and the magnetization curve is as shown in Fig. 4. The field around the central path was also mapped. It should be mentioned that the absolute value of magnetic flux and the uniformity of the field is not important in this work.

D. <u>Layout of System.</u>

Referring to Fig. 1, the source was the target and its size was determined by the size of the beam spot and the orientation of the target with respect to the beam path. The detecting system was placed at the image position, the limit of the image size being determined by the dimension of the active area of detector. Several combinations of relative distances

Fig. 3. Pole tips. Relative positions of deflecting chamber and yoke surface are shown in dotted lines. CC' is the central path.

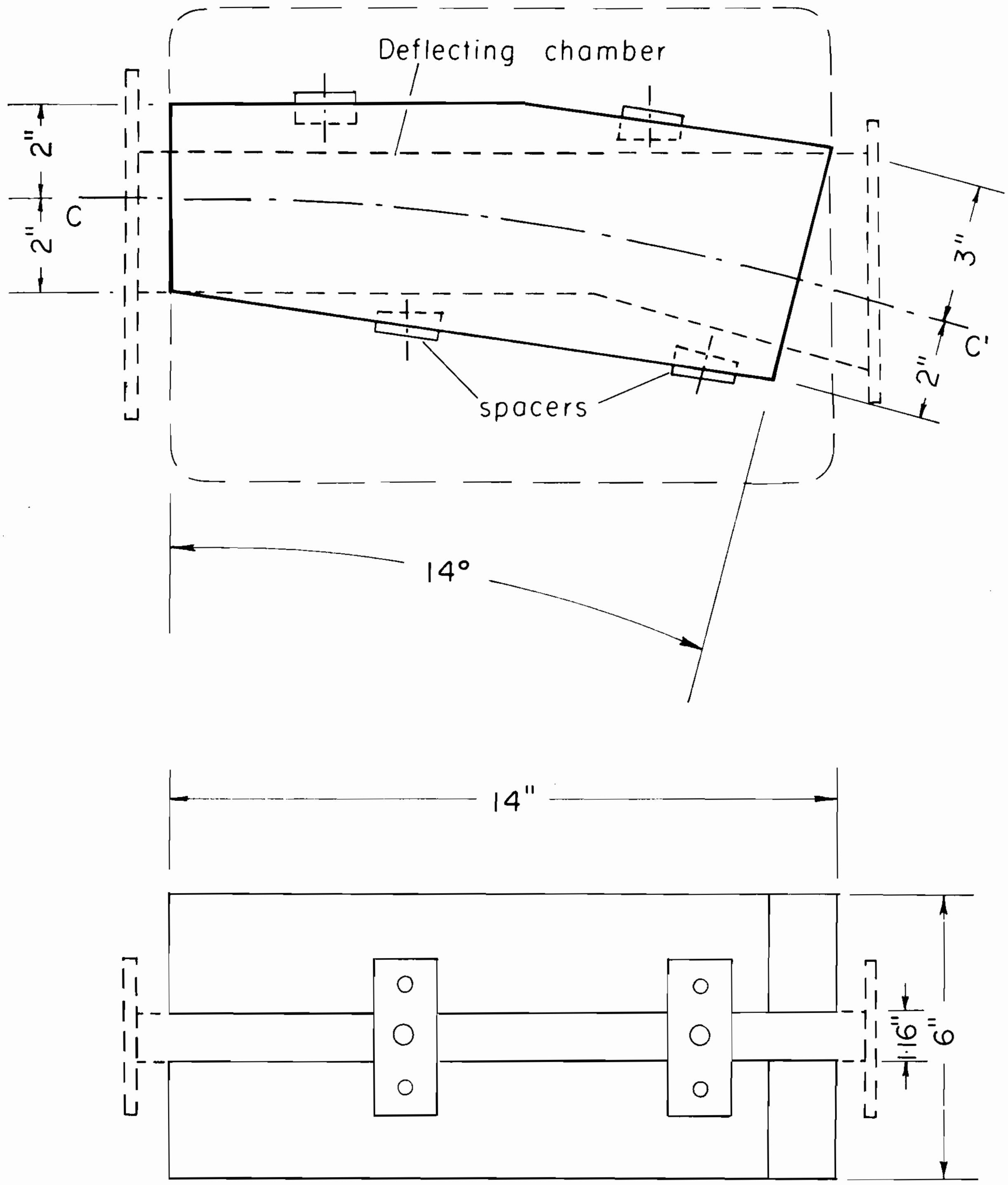

FIGURE 3

Fig. 4. Magnetization curve at central region of pole gap.

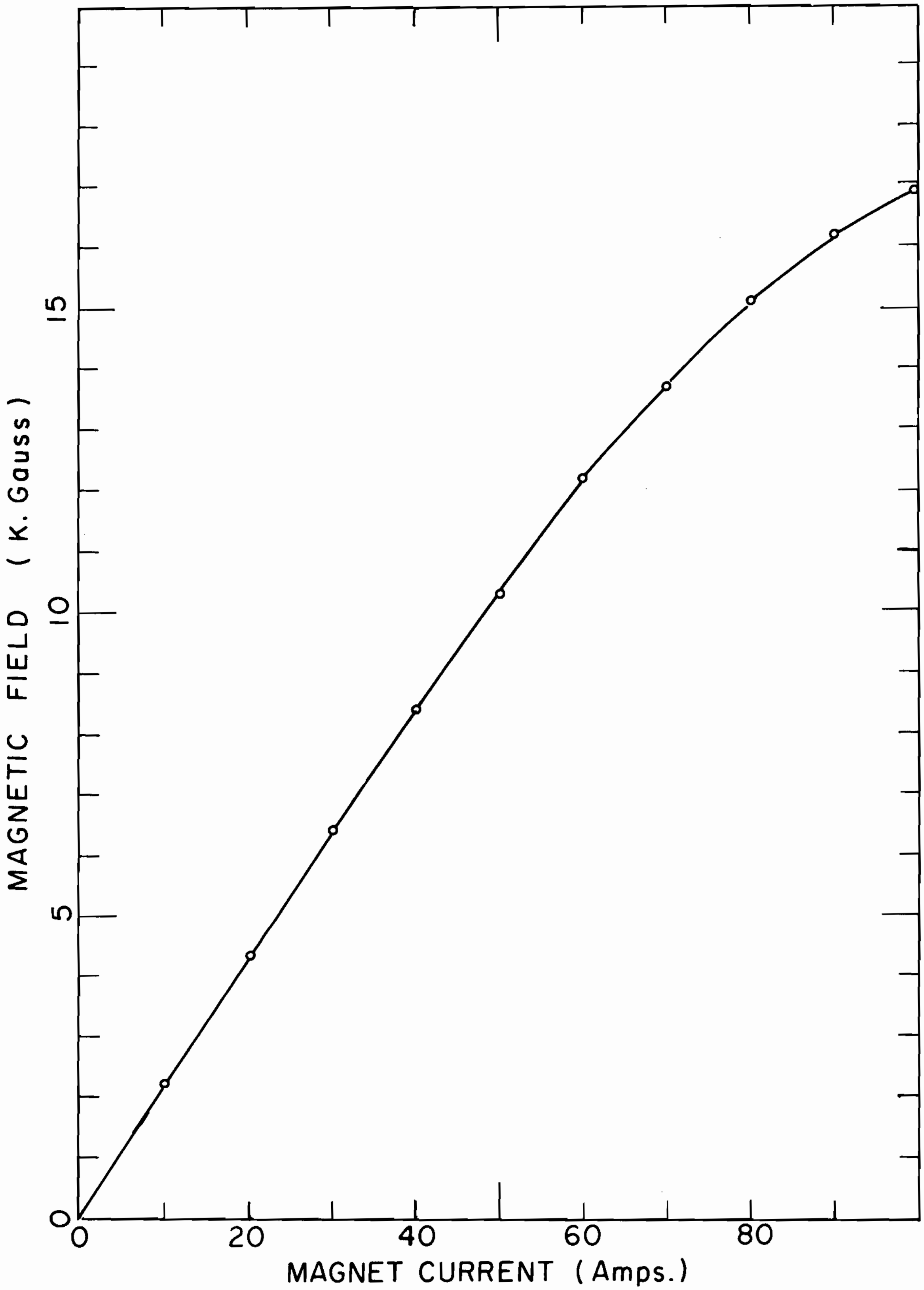
MAGNETIC FIELD (K. Gauss)
0
5
10
15
0
20
40
60
80
MAGNET CURRENT (Amps.)

FIGURE 4

between target, magnet and detector were used and their momentum separation characteristics calculated. After further considering the space requirements, the solid angle subtended by detector at target, possible effect of magnetic fringing field on counters etc., the layout as shown in Fig. 5 was chosen. Figs. 1 and 5 are equivalent to each other, and the dimensions here can be directly substituted into the equations in section II.B to get the momentum separation characteristics.

E. Particle Detector System.

The counter telescope consisted of two 200 microns thick surface barrier dE/dx solid state counters and a NaI Harshaw Line Integral counter 1.5" x 1.5" diameter. A brass collimator 5/8" thick with a 7/16" diameter hole which defined the solid angle of the detector was placed in front of the telescope. The assembly was placed in a 2.5" inside diameter iron cylinder (see Fig. 14).

The block diagram of the counting system is shown in Fig. 6. The dE/dx pulses from the preamplifiers were led to the counting room where they were clipped to 0.8 μsec. by delay line clipping and further amplified. The pulse selector unit selects the smaller of these two simultaneous dE/dx pulses, and therefore is also a coincidence unit of resolving time (2τ) twice the pulse duration. This selection process will narrow down the broadening effect of Landau spread and

Fig. 5. Geometrical layout of system. The dimensions here are used to determine the momentum selection characteristics of the system.

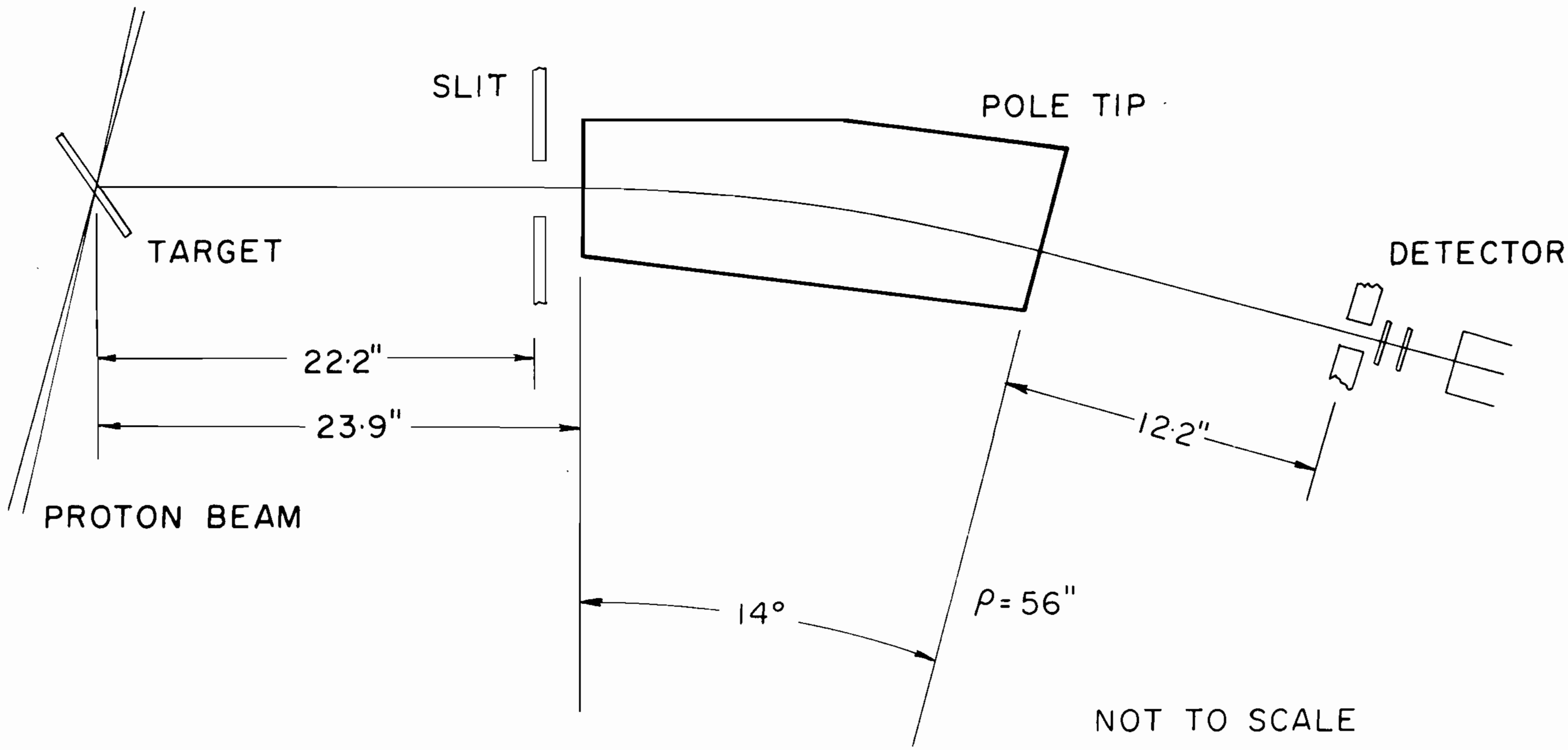

SLIT
POLE TIP
TARGET
DETECTOR
22·2"
23·9"
12·2"
PROTON BEAM
14°
ρ = 56"
NOT TO SCALE

FIGURE 5

Fig. 6. Block diagram of counting system.

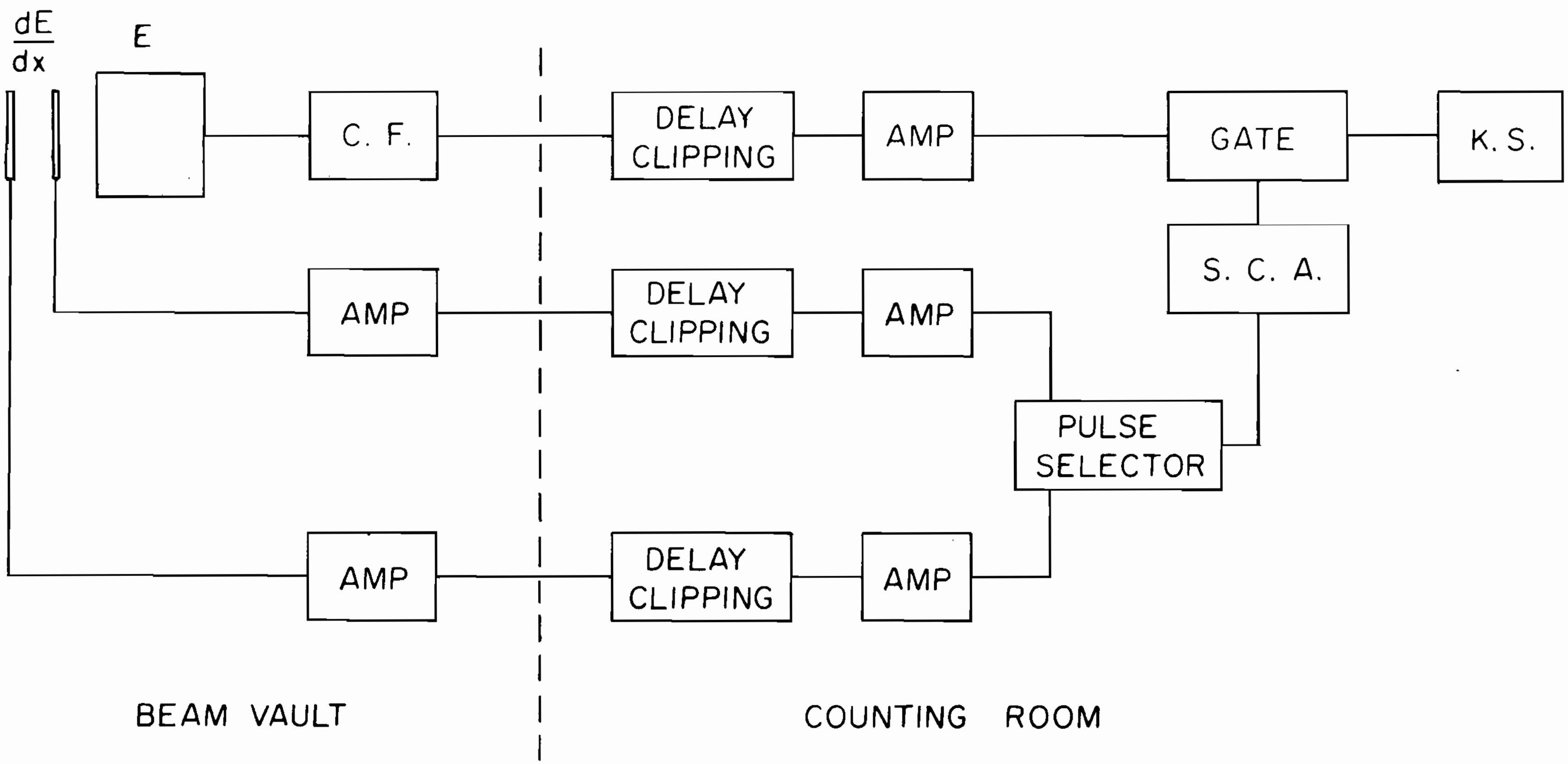
dE/dx
E
C. F.
AMP
AMP
DELAY CLIPPING
DELAY CLIPPING
DELAY CLIPPING
AMP
AMP
AMP
GATE
K. S.
S. C. A.
PULSE SELECTOR
BEAM VAULT
COUNTING ROOM

FIGURE 6

will give better particle separation (Igo 1954). The output of the selector is fed to a single channel analyser, the output of which is used to open the gate for the total energy pulses which were also clipped to 0.8 μsec. to be analysed by the multichannel analyser.

F. Particle separation of system.

By substituting the values of the geometrical dimensions in Fig. 5 into equations (II-1), (II-2) and (II-3), and assuming

$X_{omax} = -X_{omin} = 0.2''$ (corresponding to source size)

$X_{max} = -X_{min} = 0.22''$ (corresponding to detector collimator),

the expression of $S_{max}^{(n)}$ and $S_{min}^{(n)}$ can be derived and are plotted in Fig. 7.

To set the design magnet to the proper operating conditions, the magnet current required for elastically scattered protons to travel along the central path was first determined. This was done by setting the analysing slit to 0.1" on the central path, placing another 0.1" slit at the center of the detector collimator, and adjusting the magnet current so that elastically scattered protons passed through the centers of both slits. The second slit was then removed, and the upper and lower limits of magnet current for which the elastically scattered protons were detected, were measured.

Fig. 7. Momentum selection characteristic curves of the system.

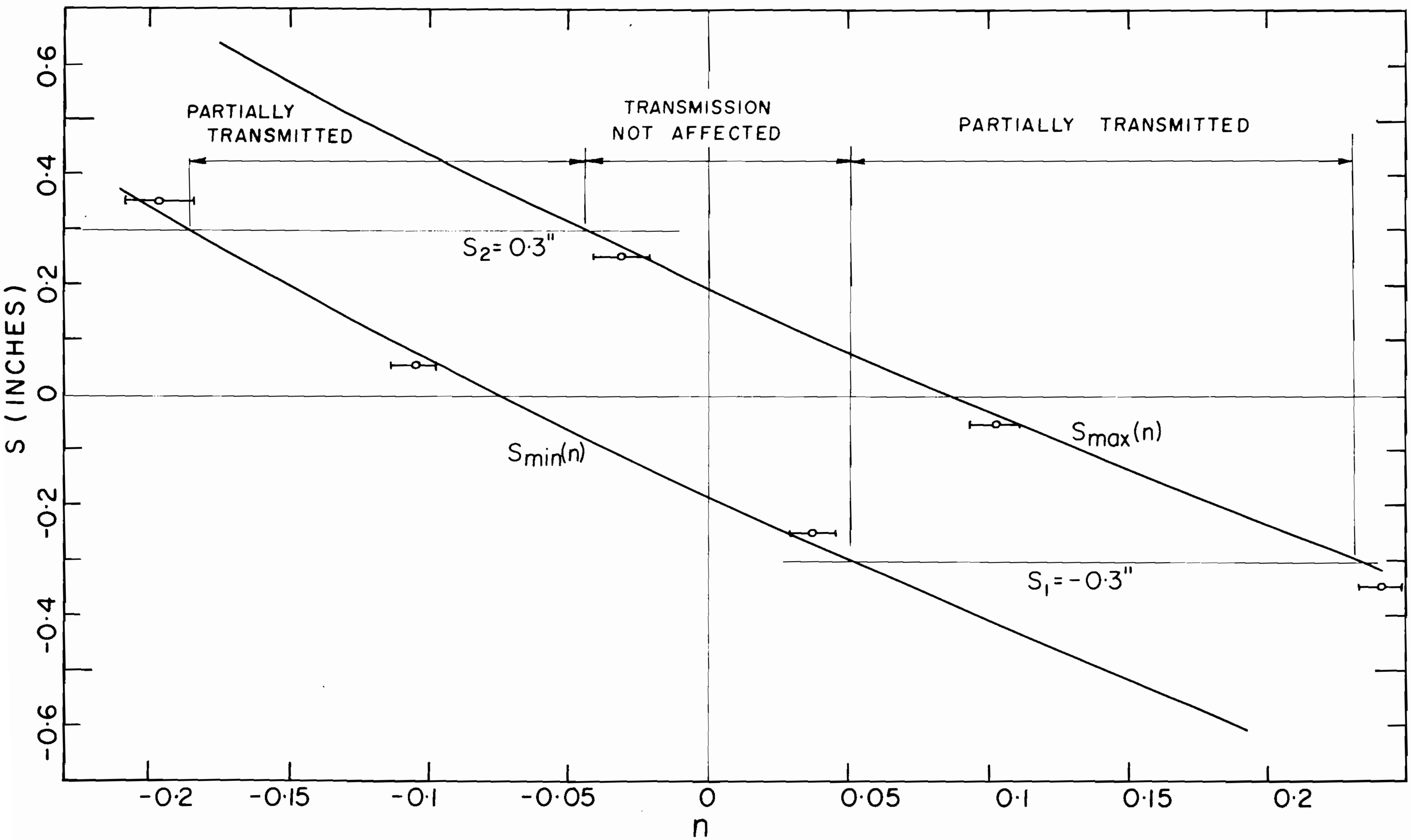

PARTIALLY TRANSMITTED
TRANSMISSION NOT AFFECTED
PARTIALLY TRANSMITTED
S₂= 0·3"
S₁= -0·3"
Smax(n)
Smin(n)
S (INCHES)
0·6
0·4
0·2
0
-0·2
-0·4
-0·6
-0·2
-0·15
-0·1
-0·05
0
0·05
0·1
0·15
0·2
n

FIGURE 7

From this, the n values could be determined. This process was repeated for a 0.1" wide analysing slit set at $\pm 0.3"$ from the central path. The results are shown in Fig. 7 and agreement with the calculated curve is quite good.

With an analysing slit opening of say from -0.3" to + 0.3", the momentum selection characteristics can be obtained by drawing the two straight lines corresponding to $S_1 = -0.3"$ and $S_2 = 0.3"$ as shown in Fig. 7. The regions of total and partial transmission can then be estimated. The selected momentum range will correspond to different energy ranges for protons, deuterons and tritons. For magnet current settings, for which the 80 Mev deuterons and 80 Mev tritons travel along the central path, the transmission of protons, deuterons and tritons is shown in Fig. 8.

From these diagrams, it can be seen that it is possible to study deuterons over quite a considerable range of energy with a complete absence of protons in this energy range but with some triton background. (Also, when studying high energy tritons, some deuterons will inevitably be present). A dE/dx gating will then further select the desired particles.

To test the particle separation system, natural graphite was used as a target. The dE/dx pulses from the pulse selector were fed directly to the multichannel analyser, and the size of these pulses was used to identify the

Fig. 8. Transmission efficiencies of protons, deuterons and tritons of different energies for (a) 80 Mev deuteron, and (b) 80 Mev triton travelling along central path.

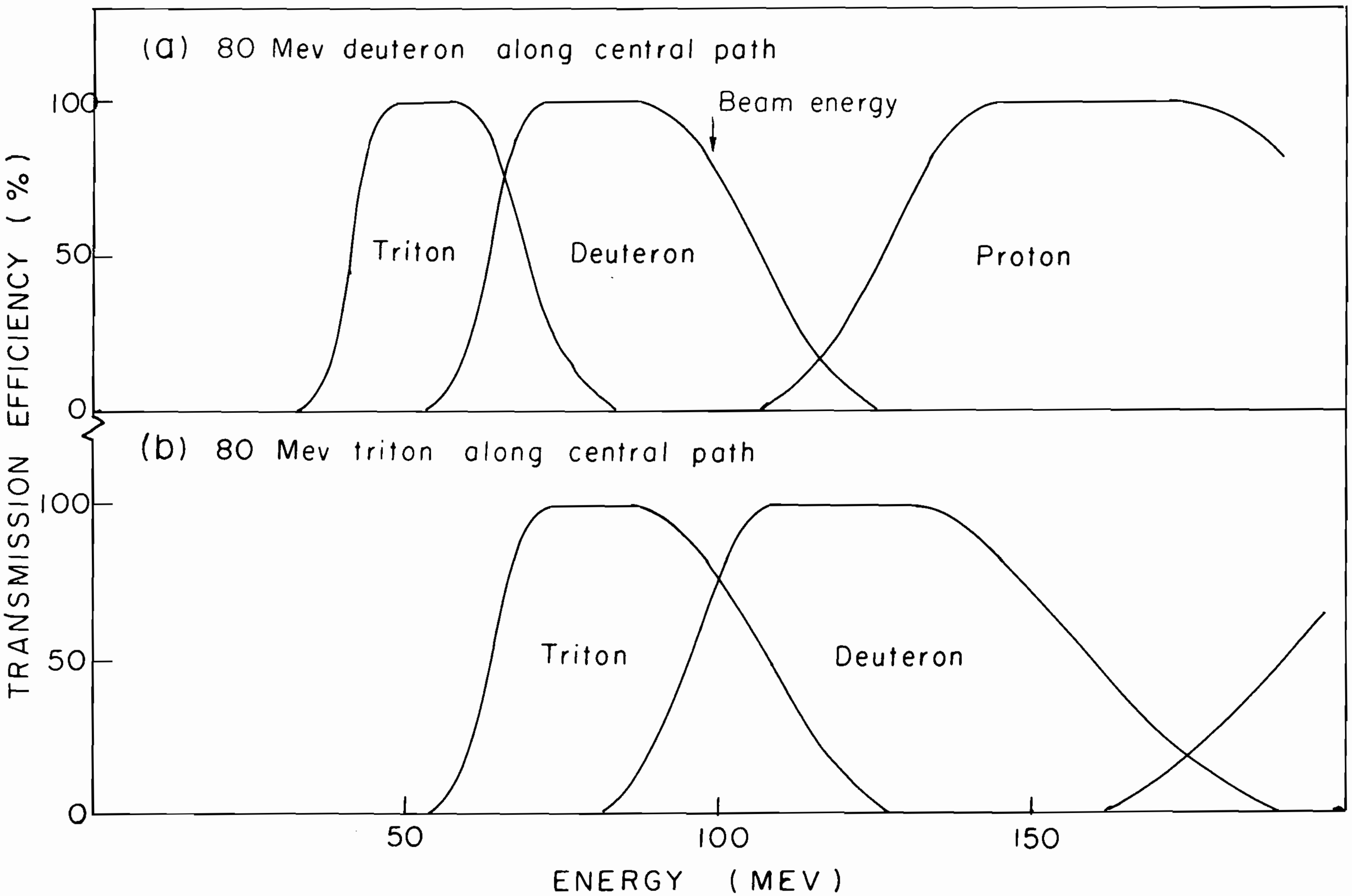
(a) 80 Mev deuteron along central path
Beam energy
Triton
Deuteron
Proton
(b) 80 Mev triton along central path
Triton
Deuteron
TRANSMISSION EFFICIENCY (%)
100
50
0
50
100
150
ENERGY (MEV)

FIGURE 8

particles. The analysing slit was set from -0.3" to +0.3". The energy spectra of the dE/dx pulses were taken for each of three magnet current settings where the central path corresponded to 90 Mev protons, 80 Mev deuterons and 80 Mev tritons. These spectra are shown in Fig. 9, and the relative spacing of these curves is arbitrary.

From curve B, corresponding very closely to the performance of the system as finally set up for the (p,d) experiments, it can be seen that the ratio of number of deuterons to tritons detected is roughly ten to one, and no protons could be detected. Most of the tritons will be on the lower side of the energy window, but a few will have sufficiently high energy to be present in the deuteron energy spectrum. To gate these high energy tritons out completely would require a low upper window setting in the dE/dx single channel analyser which would inevitably exclude an appreciable number of deuterons. However, the high energy tritons are few because of the low production cross section, and the actual number detected is further reduced by the low transmission efficiency. Therefore, the upper window of the dE/dx single channel analyser was set so that very few deuterons would be excluded (at about channel 30 for curve B in Fig. 9).

For the study of tritons, curve C in Fig. 9 indicates that a simple dE/dx gating may still include sufficient

Fig. 9. dE/dx spectra with magnet current settings for 90 Mev protons (Curve A), 80 Mev deuterons (Curve B) and 80 Mev tritons (Curve C) to travel along central path.

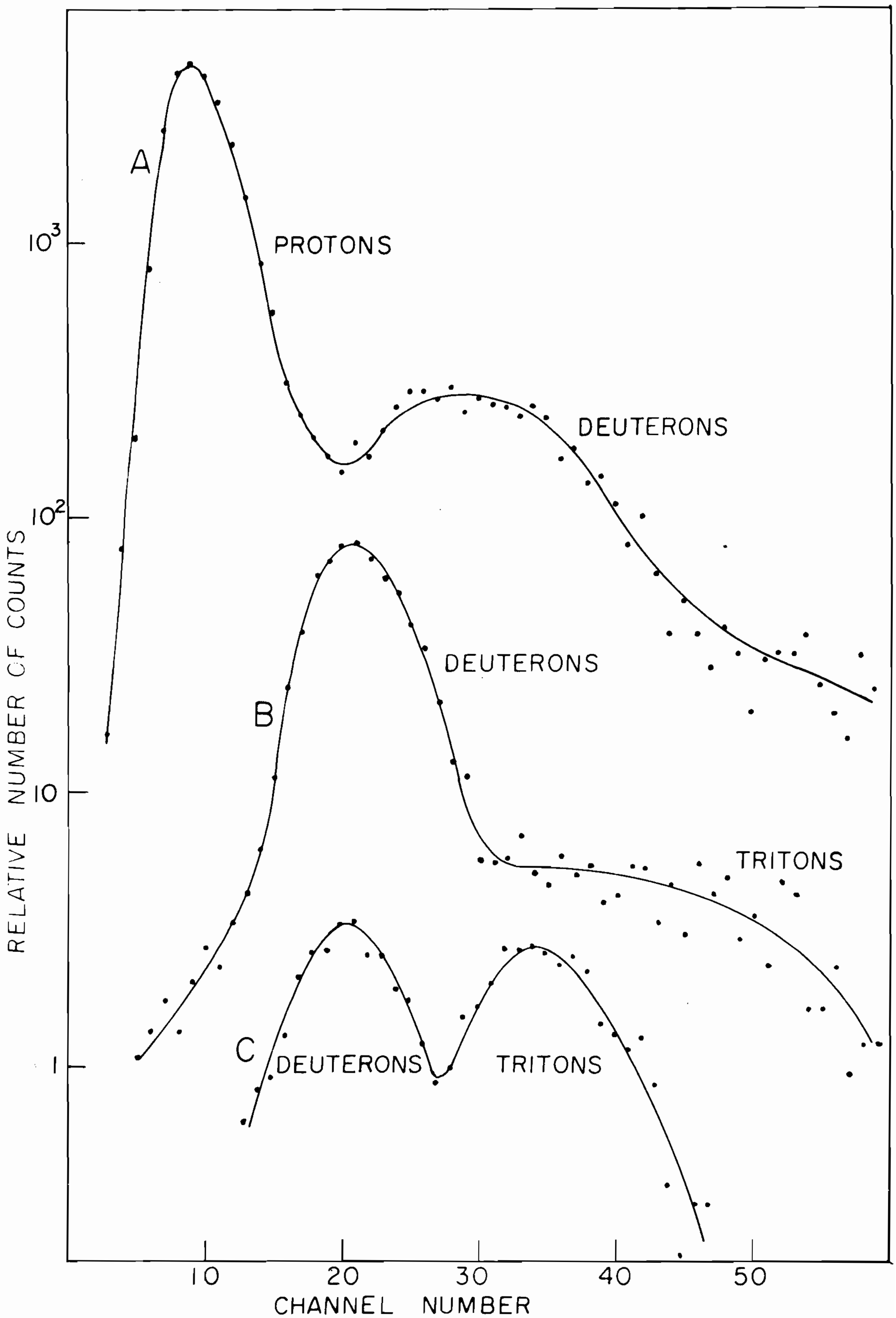
A
PROTONS
DEUTERONS
B
DEUTERONS
TRITONS
C
DEUTERONS
TRITONS
10^3
10^2
10
1
RELATIVE NUMBER OF COUNTS
10
20
30
40
50
CHANNEL NUMBER

FIGURE 9

deuterons to introduce appreciable deuteron background. This background could be reduced by narrowing down the analysing slit opening or by using a larger deflecting angle.

III. EXPERIMENTAL PROCEDURE AND TREATMENT OF DATA.

A. Set-up for large angle ($>24^{\circ}$) measurements.

The scattering chamber had proton beam entrance and exit ports of 2" inside diameter. The cover of the chamber could be rotated with respect to the body of the chamber and had a scattered particle exit port (3" inside diameter) at 20° to its plane. Therefore, it was possible to cover the angular region of laboratory scattering angle from 20° to 160°. The target mounting system inside the chamber could be rotated about the axis of the cover so as to give the target the proper orientation with respect to the proton beam and the selected direction of scattering. The target position, the axis of the chamber and the axis of the proton entrance and exit ports were aligned to 1/16".

The chamber was supported by a frame at the proton entrance and exit ports such that the whole chamber could be rotated about the proton beam path. In this way, the scattered particles observed could be confined to a horizontal plane. This assembly was mounted on a pillar which was bolted onto the floor. The axis of the pillar was aligned vertically and the center of the target (the beam spot position) was checked to lie within 1/16" of this axis.

The magnet assembly was placed on a carriage pivoted on the supporting pillar. The position of the magnet was adjusted to satisfy the requirements that the pole surface should lie in a horizontal plane with the center of the pole gap in the same horizontal plane as the proton beam, and that the scattered particles should enter the magnet with normal incident angle to the pole face edge at design position.

The deflecting chamber is shown in Fig. 10. The walls for the section between the pole tips are 0.08" thick and the verticle inside space was 1" apart. The brass analysing slit was 5/8" thick, sufficient to stop the most energetic protons. A collimator slit with horizontal sides of 0.5" vertical separation was placed before the analysing slit to reduce the scattering of the particles from the chamber walls. The entrance of the chamber was connected directly to the scattering chamber. The exit window was a 6.75" wide 0.75" high slot covered with a 0.0005" thick mylar foil.

The experimental set-up is shown in Fig. 11. Aluminium foils of 0.001" thick were used to separate the chamber vacuum from the cyclotron and the Faraday Cup vacuum. The proton beam was then focused at the target position and formed a spot not larger than 0.2" diameter. Direct beam exposure of photographic plates (Land Polaroid Film Packets Type 52) were made at the entrance port, the target position and the exit port to ensure its direction and position.

The Faraday Cup assembly had a separate vacuum pumping system and the pressure inside was always less than 0.1 micron. The cup was made of a 3.5" diameter brass tube

Fig. 10. Deflecting chamber.

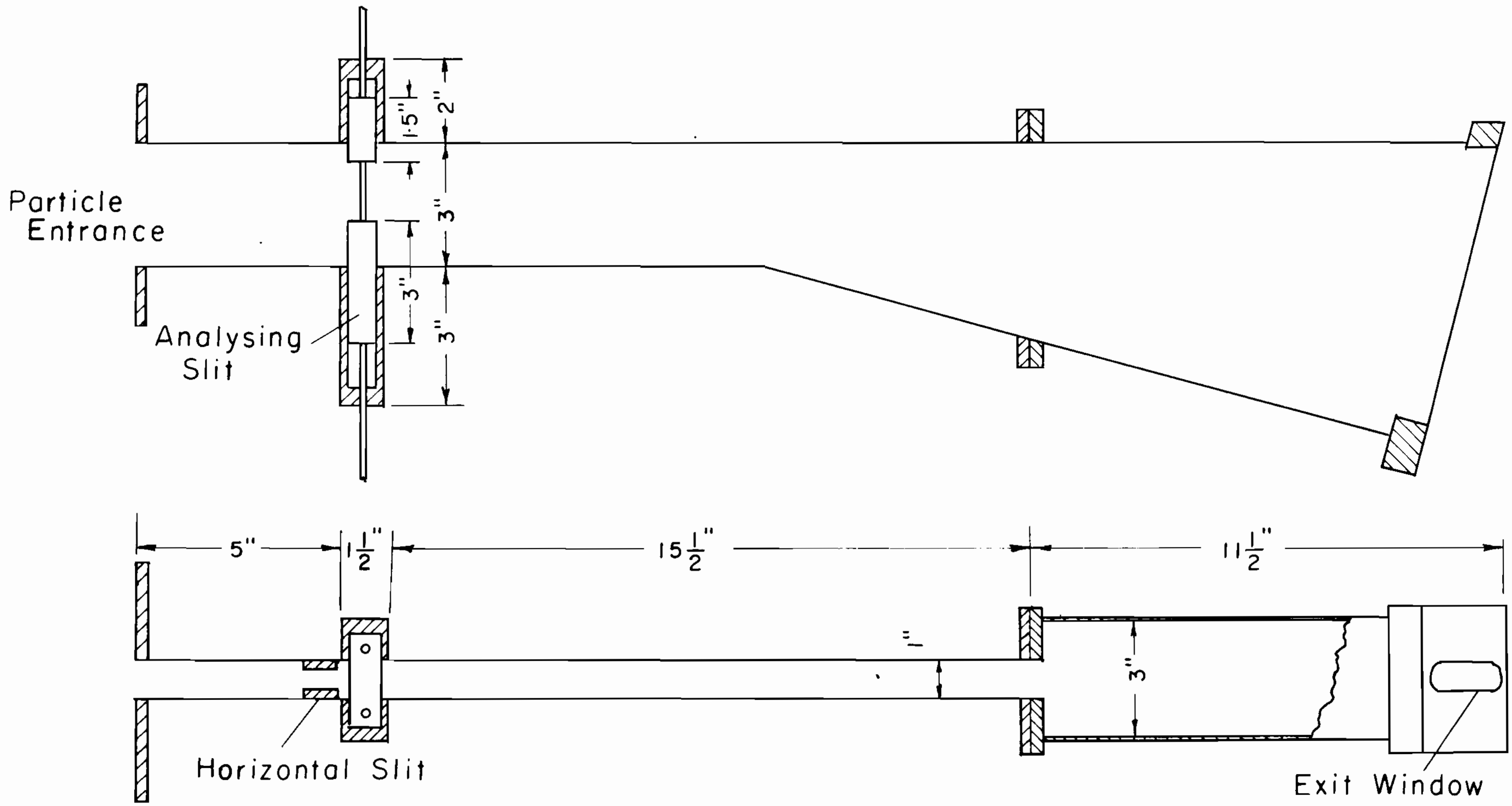

Particle
Entrance
Analysing
Slit
1·5"
2"
3"
3"
3"
5"
1 1/2"
15 1/2"
11 1/2"
1"
3"
Horizontal Slit
Exit Window

FIGURE 10

Fig. 11. Set-up for large angle ($>24^{\circ}$)
measurements.

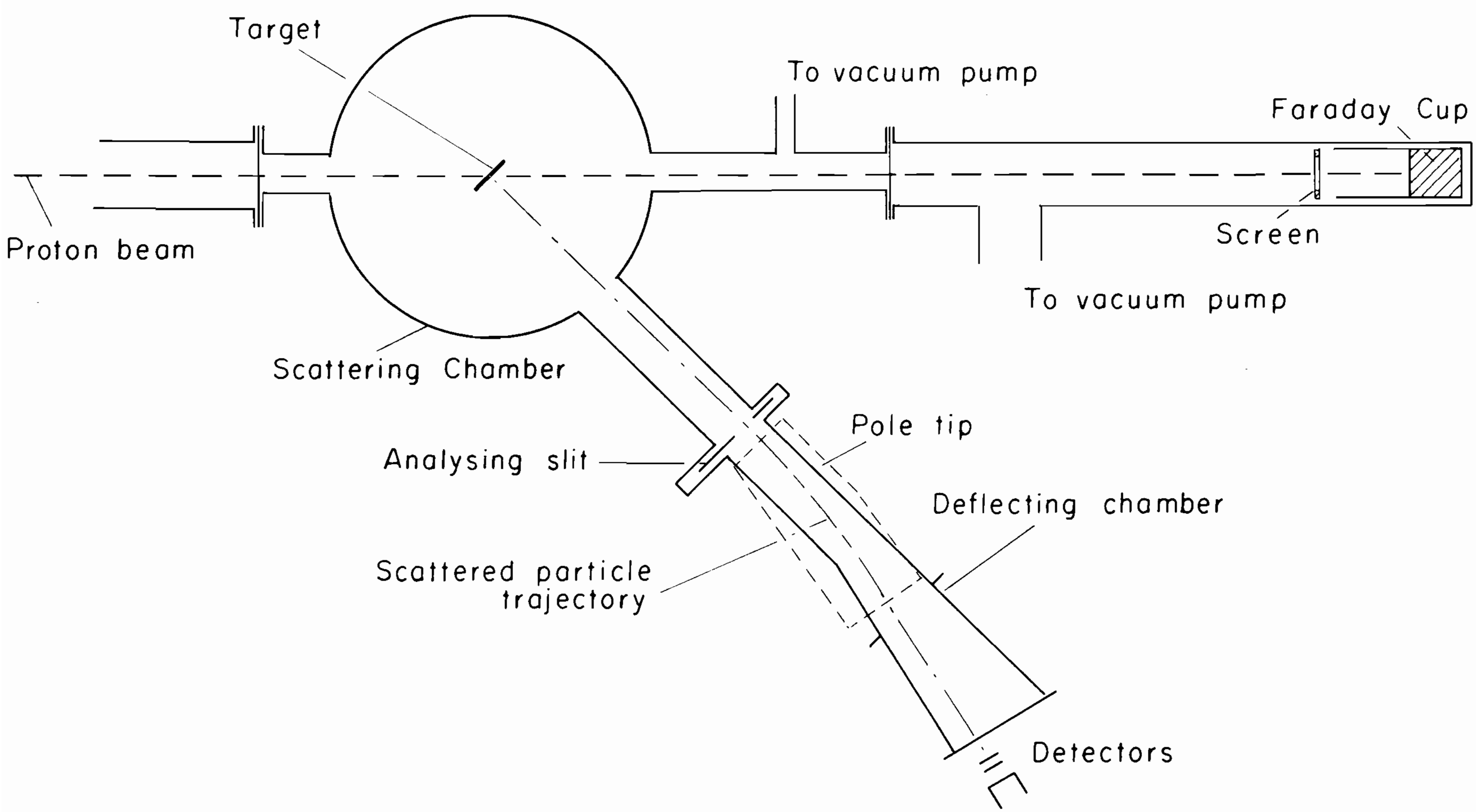

Target
To vacuum pump
Faraday Cup
Proton beam
Screen
To vacuum pump
Scattering Chamber
Pole tip
Analysing slit
Deflecting chamber
Scattered particle trajectory
Detectors

FIGURE 11

7" long and had 3" thick araldite plastic at its bottom to stop the beam. Plastic was chosen because of its low yield of background neutrons. A screen was placed in front of the cup, and a potential of 300 volts positive or negative could be applied to it to check the possible error introduced by ionization of residual gas and secondary electrons. To ensure that the cup intercepted the entire beam, a photographic exposure of the beam was taken at the position of the cup and the size was found to be less than 1.25". With these precautions, the possible error introduced should be less than 2%.

The charge collected by the Faraday cup was fed to an electrometer tube integrator unit (Lee 1960) which is calibrated to better than 2%. The relative accuracy of this unit should be better than 1%.

B. Set-up for small angles ($<24^{\circ}$)

When the investigation was completed down to 24° with the scattering chamber described in the last section, a new scattering chamber which could be used to scattering angles of almost zero degree was designed and built. The proton entrance port of this scattering chamber had an inside diameter of 2", and could be connected directly to the beam pipe. The exit window for both transmitted beam and scattered particles was a 2" high horizontal slit of azimuth -100° to 100° with respect to the exit direction of the proton beam. The slit was covered with 0.002" thick mylar foil which was sufficient to withstand the atmospheric pressure. The target mounting system could be rotated about the chamber axis as with the previous chamber.

This scattering chamber was then placed at the same position as the previous one and the alignment of beam spot, the target position, the axis of the supporting pillar and the position of the magnet assembly were checked. The deflecting chamber in this case had an entrance window of 0.0005" thick mylar, and was kept under vacuum during the experiment.

For angles between 15° and 24°, the set-up was as shown in Fig. 12. But for angles lower than 15°, the magnet assembly was moved to the other side of the scattering chamber and a plexiglas block was used to stop the beam as shown in Fig. 13. This change of side was necessary because the stopping of the beam at the exit created large γ ray and neutron backgrounds and the NaI counter could not be adequately shielded against these if placed on the normal side. The cross section measurements on either side of the scattering chamber at the same scattering angle showed no deviation.

For the small angle measurements, the Faraday cup could not be used because of its space requirements. Therefore, another counter telescope placed at a scattering angle

Fig. 12. Set-up for measurements between 15° and 24°.

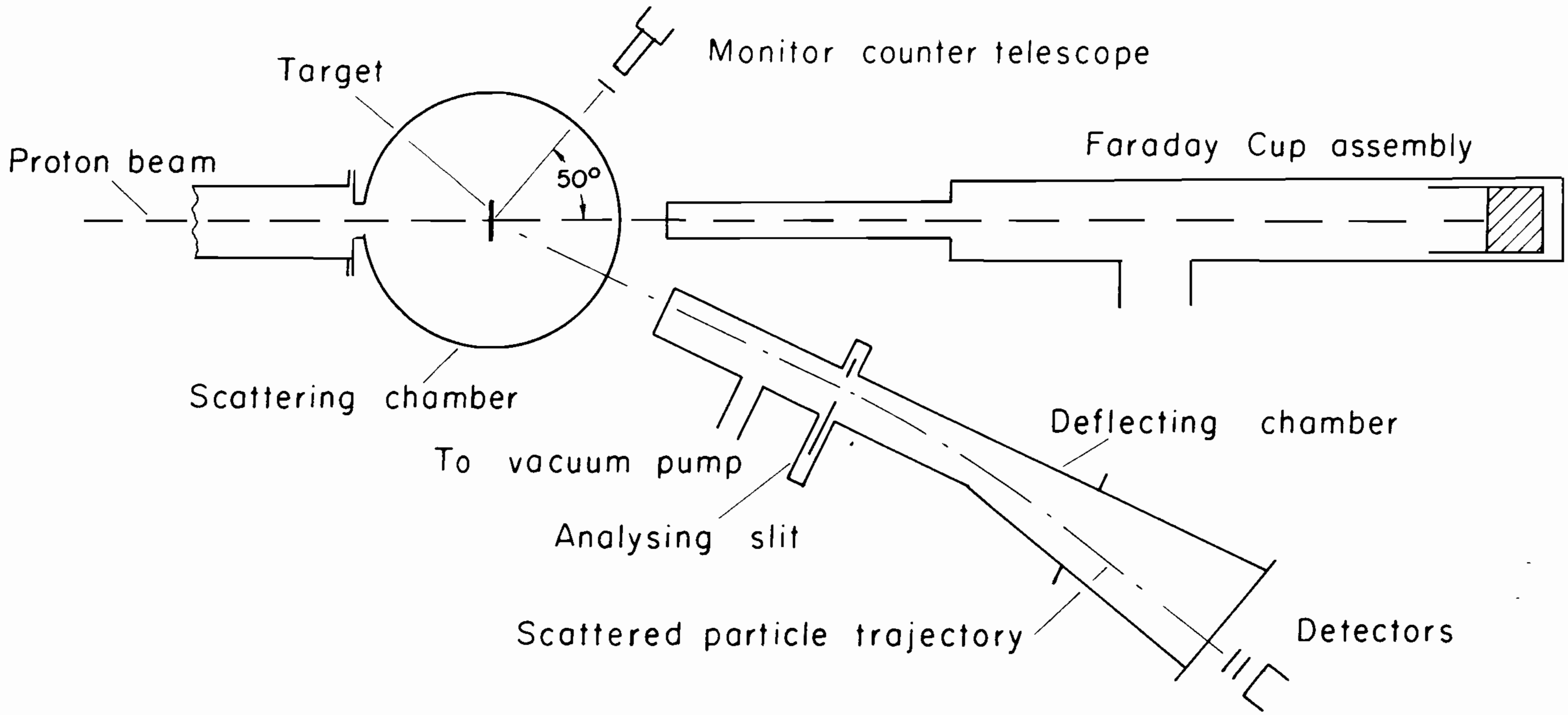
Monitor counter telescope
Target
Proton beam
50°
Faraday Cup assembly
Scattering chamber
Deflecting chamber
To vacuum pump
Analysing slit
Scattered particle trajectory
Detectors

FIGURE 12

Fig. 13. Set-up for measurements less than 15°.

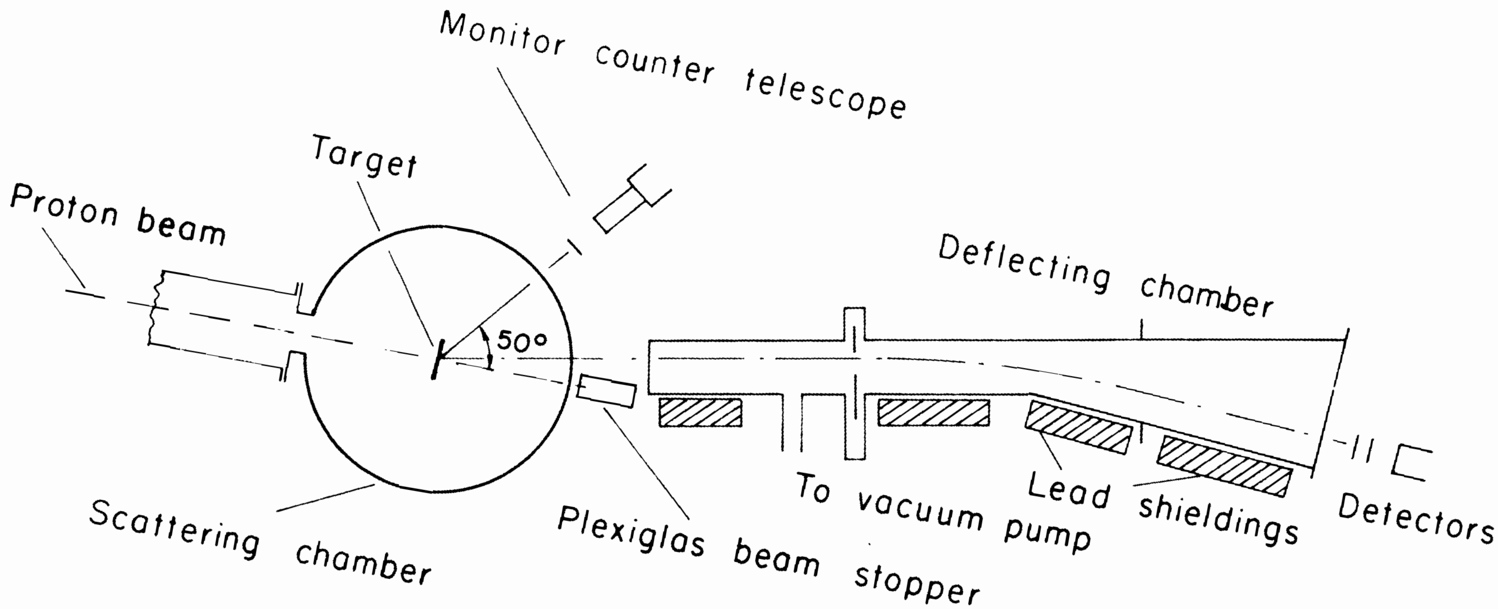
Monitor counter telescope
Target
Proton beam
50°
Deflecting chamber
Scattering chamber
Plexiglas beam stopper
To vacuum pump
Lead shieldings
Detectors

FIGURE 13

of 50^{o} as shown in Fig. 12 was used as the beam current monitor. This counter telescope (Mark 1965) consisted of plastic dE/dx and E counters. The processing circuitry consisted of a fast coincidence circuit ($2\tau = 20 \times 10^{-9}$sec.), a fast gate (open time 50×10^{-9}sec.), and a pulse shaping circuit. The current pulses from the counters were fed to the coincidence circuit and the output from this was used to open the gate. The E-pulse from the gate was fed to the pulse shaping circuit and then to a second multichannel analyser. The area under the most distinct peaks (the elastic and the first excited state proton peaks) were then integrated to give the relative number of protons collected. At about 24^{o}, both Faraday cup and counter monitoring were used. In this way, the angular distribution curves obtained at small angles were normalized to the other data. Through this angular range, the beam current used varied over a factor of five, but the coincidence rate of monitor counter outputs was kept relatively constant (within 20%) by adjusting the trigger level of the E-pulses in the coincidence circuit. This minimizes the error introduced by the uncertainty in the estimation of counting losses.

C. Alignment of counter telescope.

The counter telescope was mounted on a bracket attached to the magnet. To ensure that the observed particles entered the counter telescope along the axis of the collimator, the set-up as shown in Fig. 14 was used. The front end of the counter telescope was first fixed in the design position. With the collimator A (1/8" diameter) placed at the entrance of the telescope and the analysing slit set to 0.1" wide at the design central path, the magnet current was adjusted until the energy spectrum of the NaI counter indicated that the elastically scattered protons passed the center of the collimator A. Collimator B which had a slit of 1/8" width and 1/2" long was then placed in position. With the slit in the horizontal position, the vertical position of the rear end of the telescope was adjusted such that the elastic protons would pass through this collimator as well. A spacer of suitable thickness was placed under the rear V-block which supported the telescope. In a similar way, with the slit in the vertical position, the horizontal orientation of the telescope was determined. A suitable spacer was then placed at position C to fix the position of the telescope with respect to the deflecting chamber. This alignment was checked from time to time during the course of the experiment.

D. Energy resolution and calibration.

The fringing field at the counter position was found to be about 60 gauss for a typical magnet current setting such as that corresponding to the detection of 80 Mev deuterons.

Fig. 14. Set-up for alignment of counter telescope.

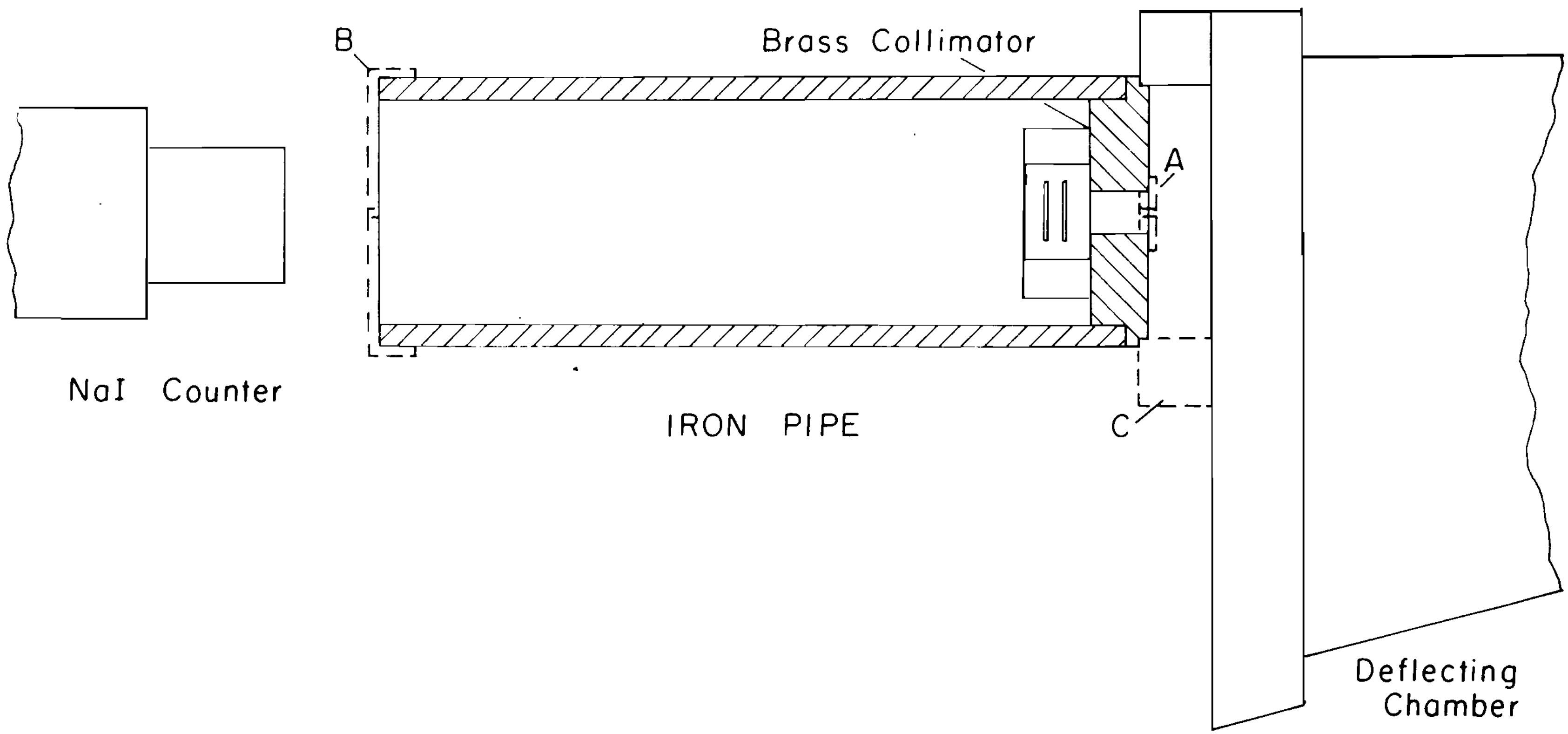

B
Brass Collimator
A
NaI Counter
IRON PIPE
C
Deflecting Chamber

FIGURE 14

Therefore, an iron pipe of 1/4" thick wall surrounding a μ-metal cylinder was necessary as a magnetic shield. However, the pulse height and the energy resolution were found to vary with the magnet current setting used and the axial orientation of the counter. Additional iron and μ-metal shielding did not seem to improve the situation. However it was found that the screen voltage of the photomultiplier required for highest pulse output was not affected by the magnet current setting or the counter orientation, and for a certain magnet current, there was always a definite orientation for maximum pulse height output. The energy resolution obtained for such orientation was the same as the best resolution obtained for zero magnet current.

Since the pulse height for particles of the same energy varied with the magnet current and the counter orientation, no absolute energy calibration was carried out. However, the linearity of light response for protons and deuterons of different energy was tested by placing absorbers of different thickness in front of the counter. The differential linearity over a 20 Mev range was better than 1%. This was sufficient to identify the levels of the residual nuclei in this work.

E. Experimental Procedure.

Before actual measurement, an aluminium plate with a 0.75" diameter hole was placed at the target position such that the center of the hole coincided with that of the beam spot. By making certain that there were no scattered particles, the position and focusing condition of the beam was ensured. With target in position, the analysing slit was set to 0.1" at the central path position, and the magnet current for the transmission of elastic protons was measured. From this measurement, the magnet current for transmission of the deuterons to be studied was determined. By this procedure, possible error due to beam misalignment and magnet current adjustment was minimized.

The proton beam current collected by the Faraday cup with and without the target was then compared to that collected by another cup which was situated at an earlier position of the beam transport system and which could be swung in and out of the beam path (the standard external beam Faraday Cup monitor). In this way, the proper operation of the Faraday cup was ensured.

For large angles, measurements were made on each target before the angular position was changed. This was because of the difficulty in changing the orientation of the scattered particle exit port of the original chamber. For small angle measurements, the entire angular region was covered for each target before the target was changed. The speed of the rotating condenser of the cyclotron, which determines the number of beam bursts per second as well as average beam intensity was recorded for each measurement so that more accurate estimation of the counting losses in the counter monitor system could be made.

In the actual measurements, the analysing slit was set to design position and the single channel analyser window set across the deuteron dE/dx peak. The counting rate was low and at the forward angles, a counting rate of ten counts per second was possible. The counting times were such that the statistical uncertainty for the most prominent peak(s) was less than 2% except in the very large angular region ($>60^{\circ}$). The "cut-off" position on the energy spectrum was checked to ensure that the transmission of deuterons observed was not affected.

F. Angular resolution.

The angular resolution in this work depends on the divergence of the beam, the position and the size of the beam spot, the accuracy in determining the position of the central path, the angle subtended by the detector collimator at the target and the angular dependence of the energy of the particles observed.

From the photographic exposures of the beam taken at the target position and the exit of the scattering chamber, the total divergence of the beam was found to be about 1°. The full width at half maximum (W_1) was then approximately 0.5°.

The size of the beam spot on the target depends on the orientation of the target with respect to the beam path. In this work, this size was always less than 0.4". The alignments of the scattering chamber and the beam ensured that the beam spot fell within 1/16" of its design position. By using the procedure as described before, the deviation of the central path from the design position should be less than 0.05". The relative position of the magnet and the scattering chamber was also aligned to within 0.1". Therefore the full width at half maximum of these combined effects (W_2) was 0.8°.

The angle subtended by the detector collimator at the target was 0.5°, and the full width at half maximum (W_3) was therefore about 0.25°.

The angular dependence of energy of the particles observed can be estimated from equations (II.1), (II.2) and (II.3). By eliminating ϕ and putting $X_0 = X = 0$,

$$\phi_0 = 0.11\ n = 0.11\ \Delta p/p = 0.055\ \Delta E/E \qquad \text{(III-1)}$$

The energy range studied in this work was less than 7 Mev, and therefore, for about 80 Mev deuterons, ϕ_0 was less than 0.3°. This will then introduce an uncertainty of full width at half maximum (W_4) of 0.15°.

Therefore, the total full width at half maximum was taken as

$$W = \sqrt{W_1^2 + W_2^2 + W_3^2 + W_4^2} \qquad \text{(III-2)}$$

$$= 1.0^\circ$$

G. Calculation of cross section.

The differential cross section leading to a certain level of the residual nucleus is given by

$$\frac{d\sigma}{d\Omega} = \frac{NAN_0 \cos\theta \, e}{\rho t Q R \, d\Omega} \quad cm^2/sterad. \qquad \text{(III-3)}$$

where N $=$ number of counts under the peak

A $=$ atomic number of target nucleus

N_o $=$ Avagadro's number $= 6.025 \times 10^{23}$ atoms/gm. atomic wt.

θ $=$ angular deviation of target from normal incident of protons

e $=$ electron charge $= 1.6 \times 10^{-19}$ coul.

ρt $=$ thickness of target in gm/cm^2

Q $=$ charge collected in coulomb.

R $=$ detector efficiency

$d\Omega$ $=$ solid angle subtended by collimator

In calculating the cross sections, there are two distinct types of uncertainty involved -- one is the systematic uncertainty, which is same for all measurements on a given target, and the other varies from measurement to measurement.

Neglecting the efficiency of the detector system, the systematic uncertainty depends on the accuracy in determining the target thickness (ρt), the charge collected (Q) and the solid angle subtended by the detector collimator at the target ($d\Omega$). The uncertainty in the target thickness was different for each target and was less than 3% for all the target used in this work. The absolute calibration of the integrator unit for the Faraday cup beam monitor system should be better than 2% and the possible error introduced by the Faraday cup beam monitor system itself should be less than 2%. Therefore, the overall uncertainty in the determination of charge collected was taken as 3%. In the estimation of $d\Omega$, the effective area of the detector collimator at the entrance edge of the pole tip was used. This was done by projecting the detector collimator area to the entrance edge of the magnet through equations (II.1) and (II.2) with $L_o = 0$. The value of the solid angle obtained this way was found to be 2% lower than that obtained by dividing the detector collimator area by the square of the central path length. The effect of the non-uniformity of the magnetic field and the magnetic fringing field on the solid angle should be less than 2%. The slit scattering from the horizontal collimator in front of the analysing slit, from the analysing slit itself and from the detector collimator was estimated by the method developed by Burgh and Smith (1962) and was found to be less than 1%. The overall accuracy of the value of $d\Omega$ should be better than 3%. The absolute uncertainty for each target was then taken as the linear sum of all these uncertainties and is given together with the results.

The relative accuracy of the differential cross section is different for each measurement and depends on the accuracy in the determination of the number of counts under a certain peak (N), the orientation of the target with respect to the beam path (θ) and the relative accuracy of Q and $d\Omega$. In the estimation of N, the method used in this work was to fit a gaussian distribution at the peak position. Background, which was not important in most cases, was neglected, and in cases where it might introduce appreciable uncertainty, it is discussed separately. The counting rate throughout this work was less than 10 counts per second and therefore the correction for counting loss was small (less than 1%) and therefore was neglected. Other uncertainities such as statistical error and error introduced in separation from neighbouring states were different for each level and they were discussed separately. The accuracy in the determination of θ should be better than 0.5°. The uncertainty thus introduced is equal to $-\tan\theta\Delta\theta$, and in this work, θ was always equal to or smaller than 60° and therefore this uncertainty was smaller than 1.5%. The relative accuracy of the Faraday cup beam monitor system and the integrator unit was taken as 1%. For small angle ($< 24^{\circ}$) measurements, the counter monitoring system was used and a relative uncertainty of 5% was assigned. The magnitude of $d\Omega$ should be constant if the effects of non-uniformity and magnetic fringing field are neglected. By taking these effects into consideration, the uncertainty in determination of the central path may introduce some relative error and an uncertainty of 1% was assigned to the relative magnitude of $d\Omega$. The errors discussed above were treated as the standard errors and the overall relative accuracy was taken as the square root of the sum of the squares of all the contributing factors. The relative uncertainties obtained in this way are tabulated with the results.

The detector efficiency is mainly due to the nuclear reaction of deuterons in the NaI counter, and it varies with the deuteron energy. Since at present, there is very little available data for the estimation of detecting efficiency of NaI counter for deuterons of this energy range, the correction for the detector efficiency was not included in the differential cross section calculation. Should such information become available, the correction can be applied to the tabulated results in a straight forward manner.

IV. RESULTS AND DISCUSSIONS

A. $O^{16}(p,d)O^{15}$

The targets used were water and plexiglas ($C_5H_8O_2$). The plexiglas was 164 mg/cm^2 thick. The water target was held between two mylar foils ($C_5H_4O_2$) each 0.001" thick. At atmospheric pressure, the thickness of water was about 0.04". When placed in vacuum, a vapour section appeared which occupied about one third of the upper target area and caused the target to expand so that it was perhaps 0.06" thick at the beam spot. However, enough area was provided so that no beam passed through the vapour section.

At large angles, both targets were used. When the plexiglas plate was used as the target, deuterons from both elements (O^{16} and C^{12}) were observed in the energy spectrum. However, since the Q values for the (p,d) reaction on O^{16} and C^{12} are -13.44 Mev -16.5 Mev respectively, it is possible to separate the deuteron group corresponding to the ground state of O^{15} from the deuterons produced from C^{12}. The energy spectrum of deuterons at 23.9° is shown in Fig. 15. Due to the larger recoil energy of C^{11} the separation became even better when the scattering angle increased. From this, after the subtraction of contributions from the $C^{13}(p,d)C^{12}$ reaction (always less than 5%), the differential cross section for $O^{16}(p,d)O^{15}$ reaction leading to the ground state of O^{15} was determined.

To obtain the deuteron energy spectrum from the $O^{16}(p,d)O^{15}$

Fig. 15. Deuteron energy spectrum from plexiglas ($C_5H_8O_2$) at 23.9° (lab. angle). The error bars shown are statistical uncertainties.

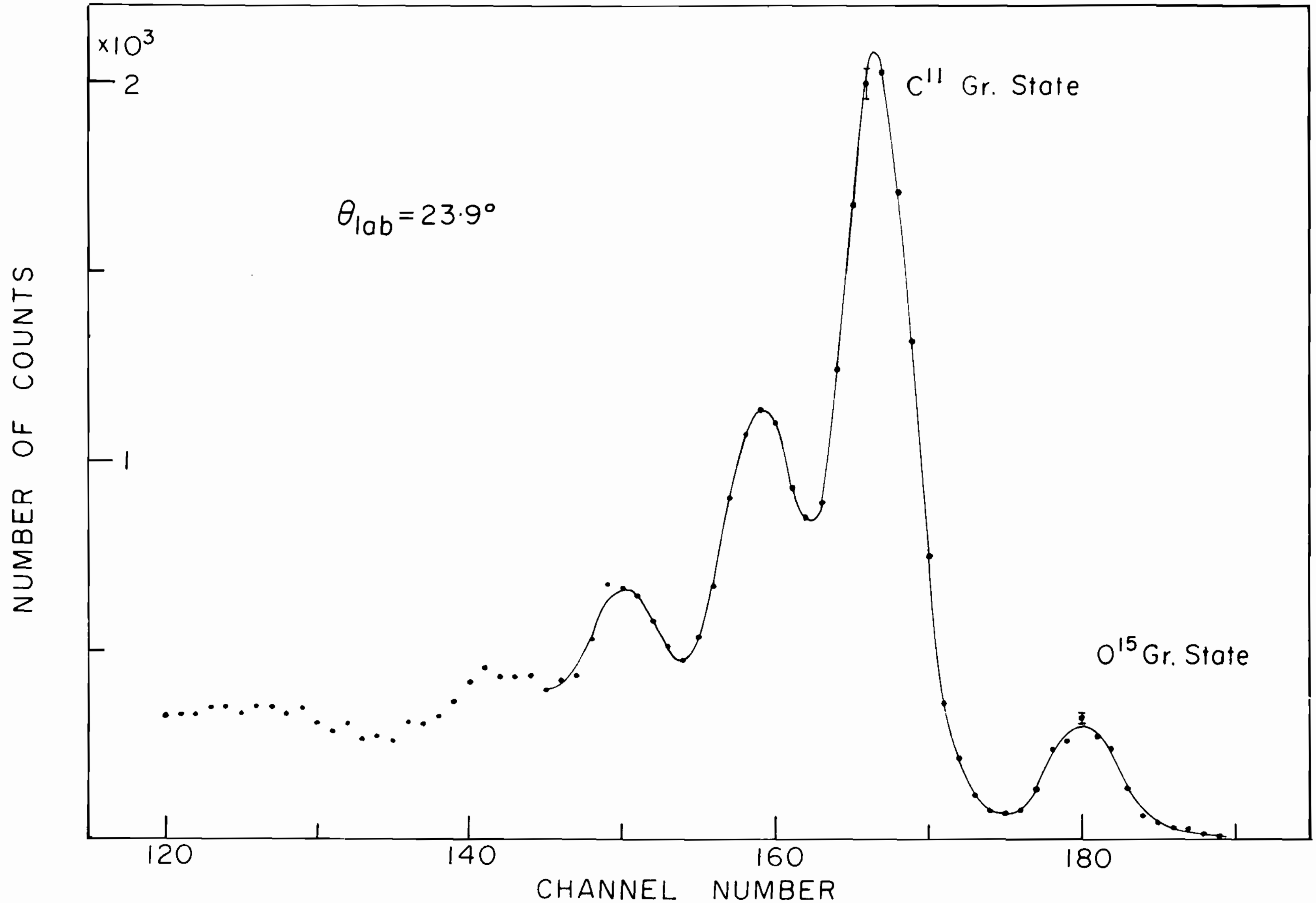

x10^3
2
1
θlab = 23·9°
C11 Gr. State
O15 Gr. State
NUMBER OF COUNTS
120
140
160
180
CHANNEL NUMBER

FIGURE 15

reaction, one method is to subtract the contribution of deuterons produced in the $C^{12}(p,d)C^{11}$ reaction from the deuteron energy spectrum obtained with the plexiglas as the target. However, since in the present case, plexiglas ($C_5H_8O_2$) has a high content of C^{12}, this method will require very good statistics in the number of counts in the energy spectra in order to yield a reasonably good deuteron energy spectrum for the $O^{16}(p,d)O^{15}$ reaction. Therefore, the water target was used in the present work.

The deuteron energy spectra from the water target at 4.4°, 23.9° and 60.0° are shown in Fig. 16. Two distinct peaks were obtained; one corresponded to the ground state of O^{15}, and the other, to an excited energy level of about 6 Mev. After the subtraction of the contribution from the carbon content in the mylar windows of the target, the ratio of the number of counts under these two peaks was determined. From this the differential cross section for the $O^{16}(p,d)O^{15}$ reaction leading to the 6 Mev excited state of the residual nucleus was determined.

For small angle measurements, since the counter monitoring method was employed, only the water target was used. At 23.9°, both the water and plexiglas targets were used with both the Faraday cup and the counter monitoring systems so that the small angle measurements could be normalized to the large angle measurements. For the small angle measurements, the contribution of deuterons from C^{12}

Fig. 16. Deuteron energy spectrum from water (H_2O) at 4.4°, 23.9° and 60.0° (lab. angles). The energy level scheme of O^{15} is shown on top of diagram. The error bars shown are statistical uncertainties.

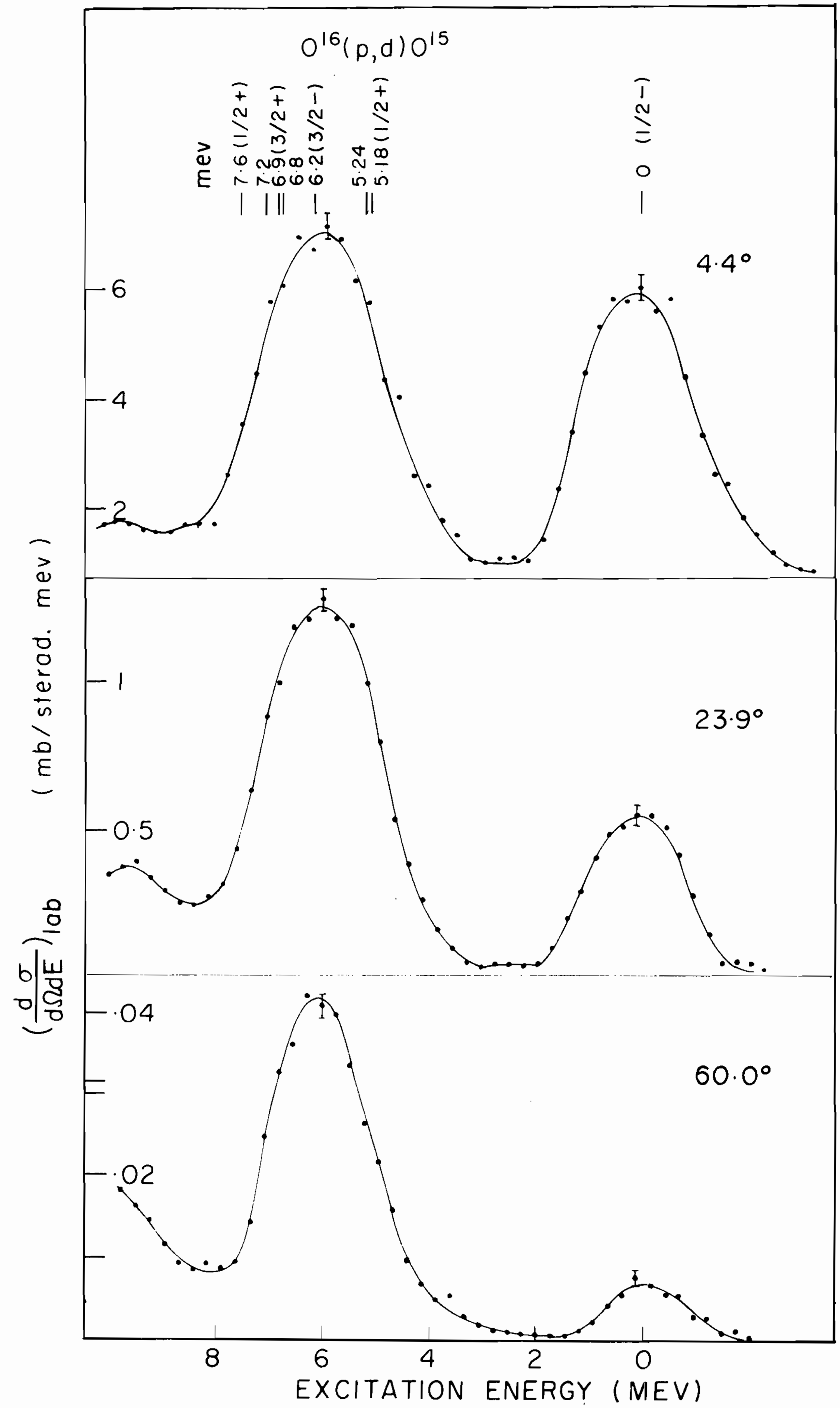

$O^{16}(p,d)O^{15}$
mev
7.6 (1/2+)
7.2
6.9 (3/2+)
6.8
6.2 (3/2−)
5.24
5.18 (1/2+)
0 (1/2−)
4.4°
23.9°
60.0°
6
4
2
1
0.5
.04
.02
$\left(\frac{d\sigma}{d\Omega dE}\right)_{lab}$ (mb/sterad. mev)
8
6
4
2
0
EXCITATION ENERGY (MEV)

FIGURE 16

was also estimated and subtracted.

The results together with the relative uncertainties are tabulated in Table 1. These results were converted to the center of mass system and are plotted in Fig. 17.

Due to the thick water target used in this work, the energy resolution obtained was about 2.5 Mev. In Fig. 16, the energy level scheme of O^{15} (Lauritsen 1962) is shown together with the energy spectra. From this, it can be seen that with the energy resolution obtained in the present work, it is difficult to estimate the contribution for each individual level at about 6 Mev. However, the deuteron energy spectrum from the $O^{16}(p,d)O^{15}$ reaction at 40 Mev (Kavaloski 1963) showed only two distinct peaks corresponding to the ground state (1/2 -) and the 6.2 Mev excited state of O^{15}, and the energy resolution obtained in that experiment was capable of resolving all the neighbouring states. The same conclusion was reached at 155 Mev (Bachelier 1964). Since the excited states observed in the pick-up reaction for a given target do not seem to change with incident energy in this energy range (Matsuda 1962), and since in this work there was no obvious broadening of the 6 Mev group as compared to the ground state group, this 6 Mev group was judged to be entirely from residual nuclei in the 6.2 Mev (3/2 -) state.

For $O^{16}(p,d)O^{15}$ results at 155 Mev, another group of deuterons corresponding to about 9.8 Mev excitation energy of O^{15} was reported. In this work, such a peak was observed at

TABLE 1

Differential cross sections of the deuteron groups from the $O^{16}(p,d)O^{15}$ reaction.

Absolute systematic uncertainty = ±8%.

Lab. Angle degrees	$(d\sigma/d\Omega)_{lab}$ (mb/sterad.)	
	0 Mev	6.2 Mev
4.4	12.6 ± 0.7	16.6 ± 0.9
6.7	12.0 ± 0.7	17.3 ± 1.0
10.2	8.36 ± 0.46	14.2 ± 0.8
13.0	5.64 ± 0.31	10.2 ± 0.6
14.8	4.21 ± 0.23	8.41 ± 0.46
18.0	2.58 ± 0.14	5.47 ± 0.30
21.4	1.67 ± 0.09	3.88 ± 0.21
23.9	1.21 ± 0.04	3.41 ± 0.11
24.2	1.17 ± 0.04	3.22 ± 0.11
28.2	660 ± 20 $\times 10^{-3}$	2.54 ± 0.09
31.5	421 ± 13	1.92 ± 0.07
34.8	388 ± 12	1.49 ± 0.05
39.2	260 ± 9	860 ± 30 x 10^{-3}
44.7	154 ± 6	572 ± 24
49.7	65.2 ± 2.7	294 ± 13
54.7	24.4 ± 1.1	206 ± 10
60.0	11.9 ± 0.6	93 ± 6
65.0	9.5 ± 0.5	72 ± 5
67.0	9.5 ± 0.5	40 ± 3
70.3	10.4 ± 0.6	45 ± 3
72.0	6.1 ± 0.5	26 ± 3
79.9	1.5 ± 0.2	8.2 ± 1.1

Fig. 17. Angular distributions for deuteron groups produced in $O^{16}(p,d)O^{15}$ reaction.

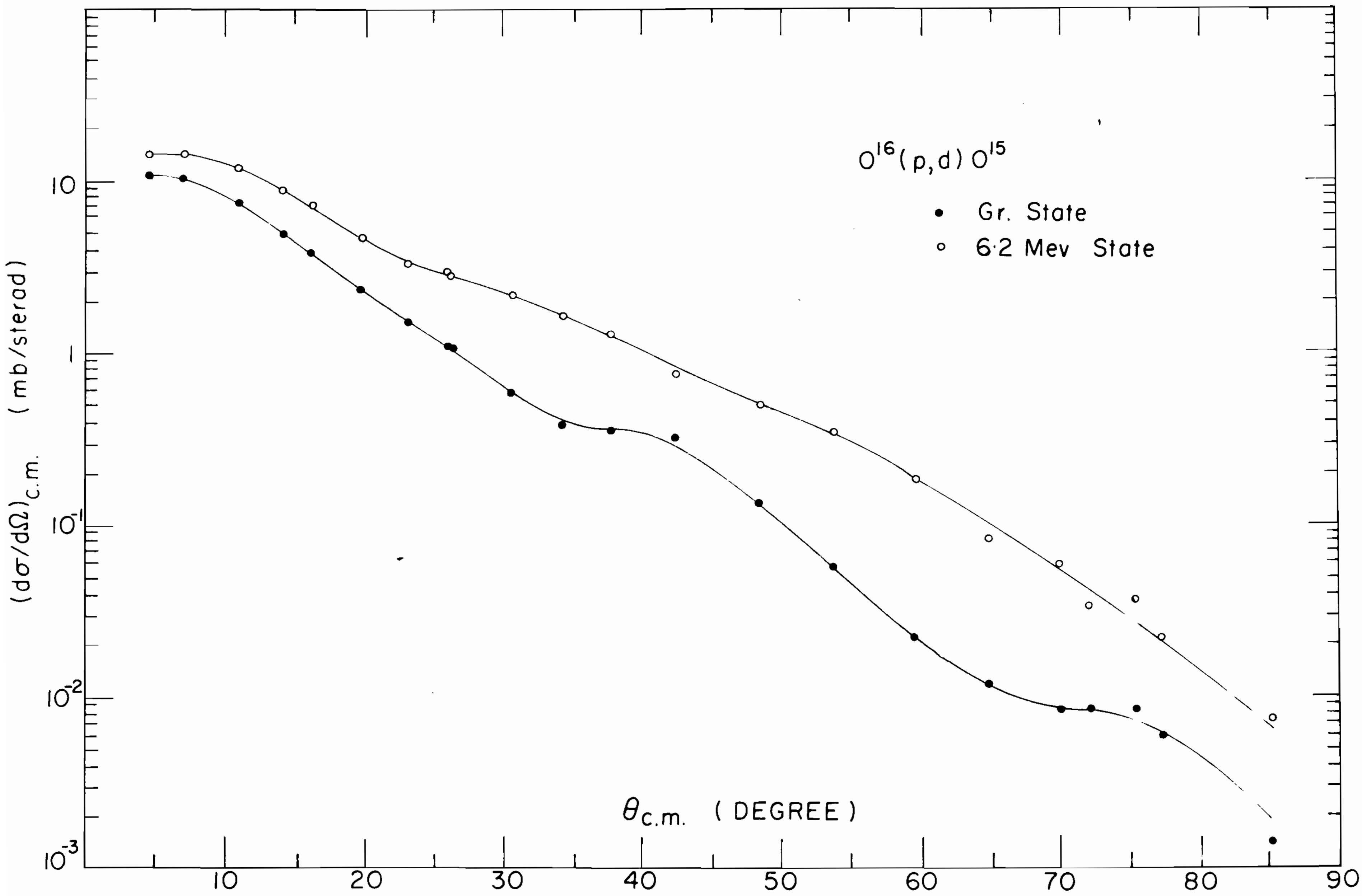
$O^{16}(p,d)O^{15}$
Gr. State
6·2 Mev State
$(d\sigma/d\Omega)_{c.m.}$ (mb/sterad)
$\theta_{c.m.}$ (DEGREE)
10
1
10^{-1}
10^{-2}
10^{-3}
10
20
30
40
50
60
70
80
90

FIGURE 17

small angles, but it was weakly excited and disappeared completely at larger angles. Therefore, the differential cross sections are not reported here.

In the shell model, the ground state of O^{16} corresponds to a closed 1p shell. In calculating the energy level scheme of different elements in the 1p shell, Kurath (1956) found that as the 1p shell was gradually filled, the spin-orbit coupling became stronger. Recently, Amit et al (1964) assumed a jj-coupling scheme and estimated the absolute binding energies of $1p_{1/2}$ and $1p_{3/2}$ neutrons in the ground state of O^{16} and obtained good agreement with experimental results (within 0.13 Mev in absolute energy and within 0.03 Mev for the energy difference between them). Accepting this jj-coupling scheme in the shell model and neglecting the interaction between the incoming particle and the core nucleus (the impulse approximation), in (p,d) reaction on O^{16} only (3/2-), (1/2-) and (1/2+) states in the residual nucleus can be obtained. These correspond to the pick-up of a $1p_{1/2}$, $1p_{3/2}$ and $1s_{1/2}$ neutrons respectively. This is in agreement with the results of this work. The deuterons corresponding to the pick-up of a $1s_{1/2}$ neutron would have energy outside the range of observation of this work and, in any case, such deuterons would have a large energy spread and it may be difficult to distinguish them from the general continuum.

The results of similar experiments such as $O^{16}(\gamma,n)O^{15}$

(Tanner 1964) and $O^{16}(p,2p)N^{15}$ (Typren 1958) showed that the residual nuclei were mainly in (1/2-), (3/2-) and (1/2+) states. However, in the observation of γ-ray de-excitation of residual nuclei from the $O^{16}(p,pn)O^{15}$ reaction at 150 Mev (Foley 1962, Rowe 1962), a small yield from 5.2 Mev and 6.9 Mev states was observed. This seemed to indicate that the O^{16} ground state had some small configuration mixing in the ds shells, but this discrepancy could also be explained by allowing a different reaction mechanism for the (p,pn) process.

The angular distribution curves in Fig. 17 show that the diffraction patterns for the two groups are quite different. In the case of the deuteron group corresponding to the pick-up of a $1p_{1/2}$ neutron, (the ground state group), a diffraction peak was observed at about 75^{o}. This was confirmed by repeating the measurements in this angular region.

The dependence of the angular distribution on the total angular momentum transfer for reactions of the same orbital angular momentum transfer has been observed recently on (d,p) reaction (Lee 1964), (d,t) reaction (Fulmer 1964) and (p,d) reaction (Sherr 1964) at low energies. In all these results, the angular distributions for the lower total angular momentum transfer had a more oscillating pattern. Recently, Lee et al (1965) carried out a distorted wave analysis and included a spin-orbit coupling term in the distorting potential for the (α,p) reaction at 18 Mev. A qualitative agreement with the experimental results was obtained. In the present work, the j-dependent effects were not very distinct but certainly observable. The nature of these effects cannot be determined until a detailed distorted wave analysis is carried out.

B. $C^{12}(p,d)C^{11}$

The target used was a natural graphite plate (98.9% C^{12} and 1.1% C^{13}), 89 mg/cm^2 thick. The deuteron energy spectra at 4.9°, 23.8° and 60.0° are shown in Fig. 18 together with the energy level scheme of C^{11} (James 1961, Freeman 1962). Four prominent peaks were observed, corresponding to residual nuclei in the ground state (3/2-) and the excited states of 2 Mev (1/2-), 4.8 Mev (3/2-) and 6.9 Mev (-). This is in agreement with the results obtained for the same reaction at 57 Mev (Matsuda 1962) and 155 Mev (Radvanyi 1962).

The energy resolution obtained was about 1.3 Mev, sufficient to separate the 2 Mev state from the ground state. The number of counts accumulated under the peak corresponding to the ground state of C^{11} for each measurement (except for angular region larger than 65°) was such that the statistical error would be less than 2%. Therefore, the possible error

Fig. 18. Deuteron energy spectrums from carbon at 4.9°, 23.8° and 60.0° (lab. angles). The energy level scheme of C^{11} is shown on top of the diagram. The error bars shown are statistical uncertainties.

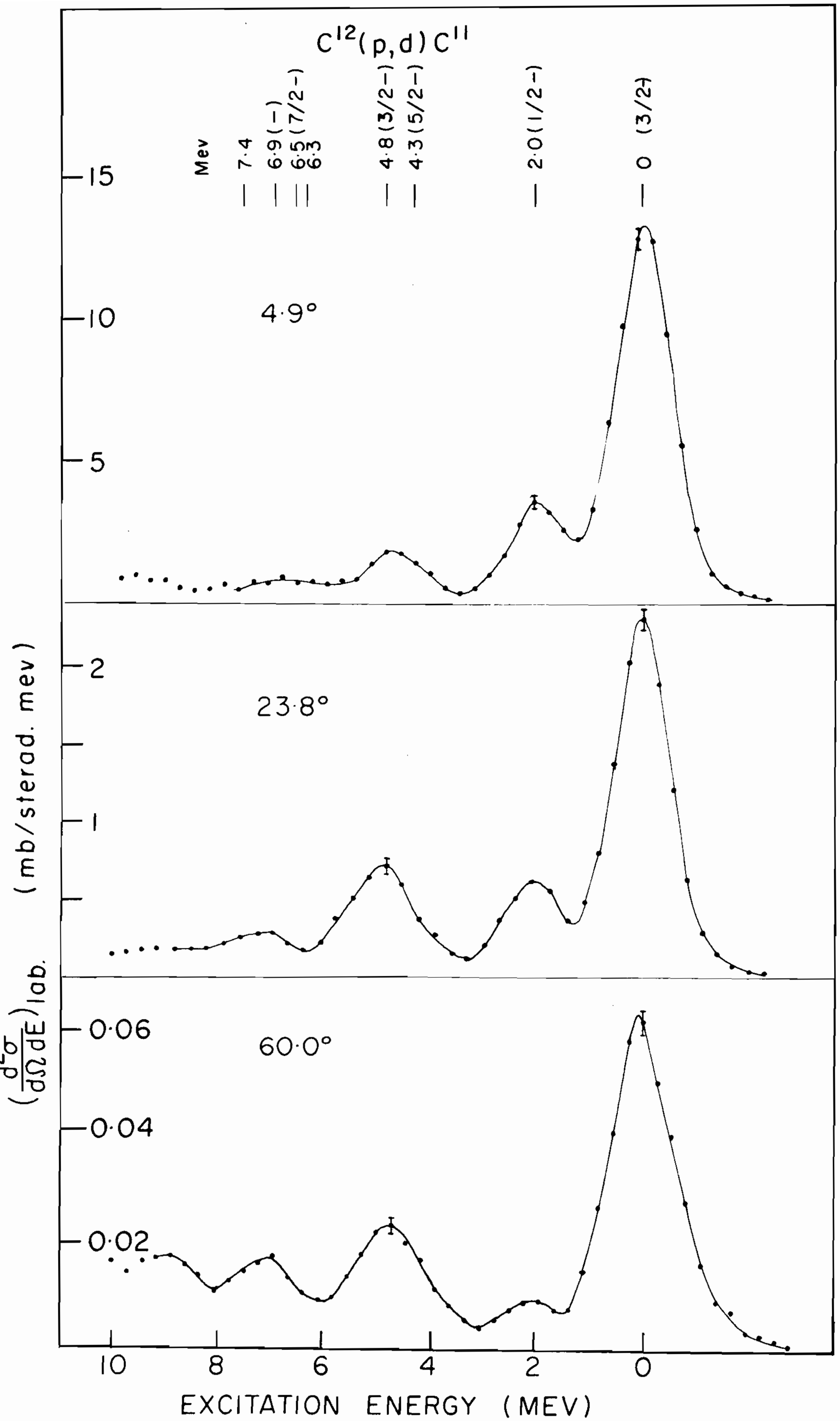

C12(p,d)C11
Mev
7·4
6·9(−)
6·5(7/2−)
6·3
4·8(3/2−)
4·3(5/2−)
2·0(1/2−)
0 (3/2−)
15
10
5
4·9°
2
1
23·8°
0·06
0·04
0·02
60·0°
(mb/sterad. mev)
(d²σ/dΩdE)lab.
10
8
6
4
2
0
EXCITATION ENERGY (MEV)

FIGURE 18

introduced in separating the 2 Mev state from the ground state would be small (less than about 5%). From the energy spectra in Fig. 18, it can be seen that the width of the deuteron peak corresponding to the 4.8 Mev excited state of C^{11} is about the same as that of the ground state peak. Therefore, the 4.3 Mev (5/2-) state of C^{11} was very weakly excited and its contribution of deuterons under this peak would be small (less than about 10%). In the calculation of the differential cross sections, this entire group was assigned to the 4.8 Mev state. The 6.9 Mev state was quite weakly excited in the forward angular region ($<15^{o}$), and in these cases, the total number of counts under the peak was estimated by fitting a gaussian at the peak position. The results obtained in this way would certainly involve a large uncertainty, and a standard error of 15% was assigned to it.

Possible background in this experiment is mainly due to the nuclear reaction of deuterons in the NaI counter, the C^{13} content of the target and possible feed through of tritons. Assuming that 15% of the deuterons entering the NaI counter will undergo some type of nuclear reaction and that the pulse height outputs from them will be uniformly distributed throughout the pulse height spectrum, the background thus introduced under any peak might contribute up to 2% of the cross section obtained in most cases, and up to 8% for the 6.9 Mev state in the forward angular region ($<15^{o}$).

Since the detector efficiency correction (mainly due to the nuclear reaction of deuterons in NaI counter) was not included in the differential cross section calculation, and that the background thus introduced was small as compared to the other uncertainties in the experiment, these backgrounds were neglected in the calculations and the uncertainties thus introduced were included in the relative uncertainties. The Q value for the $C^{12}(p,t)C^{10}$ reaction is -23.5 Mev, and should not introduce any background in most of the angular regions, but in the forward scattering angles, the most energetic tritons would appear in the energy spectrum at the position corresponding to about 7 Mev excitation energy of C^{11}. Since the 6.9 Mev state of C^{11} was very weakly excited in this angular range, even small feed-through of these high energy tritons could be important. But, the light response from tritons in a NaI scintillator is not certain, and it would be difficult to study experimentally its contribution in this case. However, the cross section for the production of high energy tritons is low, and their feed-through were further reduced by their low transmission efficiency and the dE/dx gating in the present system, the contribution of tritons should be less than 10% of the estimated total count. Since no accurate estimation of the contribution of these high energy tritons could be made, they were included in the cross section calculation, and the uncertainty thus introduced was included in the relative uncertainty. The C^{13} content of the target is small (1.1%), and its contribution in the background was neglected. The uncertainty thus introduced (taken to be 1%) was included in the absolute systematic uncertainty.

The differential cross sections are tabulated in Table 2 together with the relative uncertainties. The results were converted to the center of mass system and are shown in Fig. 19. On the same diagram, the results for the same reaction at 95 Mev (Selove 1956) are also shown. Since the energy resolution obtained in that work was about 3 Mev, those results shown would have some contribution from the first excited state of C^{11}. The agreement in the angular distributions is quite good, and the discrepancy in the absolute magnitude of the differential cross sections is due to not including the detector efficiency in this work.

For a jj-coupling scheme in the shell model, only the (3/2-) and (1/2-) states should be observed for the (p,d) reaction on C^{12}. The presence of the 2 Mev (1/2-) state indicated that some configuration mixing in the ground state of C^{12} will be necessary. The available data on the 6.9 Mev state is relatively sparse. In the $B^{10}(d,n)C^{11}$ reaction at 4 Mev, James et al (1961) obtained ℓ=1 for the transition to the 6.9 Mev state in C^{11}, and they correlated this level to the 7.3 Mev (5/2-) state in the mirror nucleus B^{11}. Should

TABLE 2

Differential cross sections of the deuteron groups from the $C^{12}(p,d)C^{11}$ reaction.

Absolute systematic uncertainty $= {+8\% \atop -9\%}$

Lab. Angle degree	$(d\sigma/d\Omega)_{lab}$ (mb/sterad.) 0 Mev	2.0 Mev
4.9	17.2 ± 0.9	3.95 ± 0.24
7.3	16.2 ± 0.8	4.06 ± 0.25
10.3	12.9 ± 0.7	2.76 ± 0.17
13.7	8.66 ± 0.45	1.90 ± 0.11
16.3	5.91 ± 0.31	1.34 ± 0.08
19.4	4.40 ± 0.23	1.02 ± 0.06
23.8	3.06 ± 0.08	701 ± 28 $\times 10^{-3}$
24.2	3.02 ± 0.08	756 ± 31
28.2	2.41 ± 0.07	448 ± 19
31.5	1.81 ± 0.05	260 ± 12
34.8	1.29 ± 0.04	154 ± 7
39.2	716 ± 21 $\times 10^{-3}$	126 ± 6
44.7	411 ± 12	91 ± 5
49.7	280 ± 8	56.5 ± 3.1
54.7	172 ± 5	27.4 ± 1.6
60.0	94 ± 3	15.1 ± 0.9
63.4	65 ± 2	8.1 ± 0.5
65.0	55 ± 2	5.7 ± 0.4
67.7	39.2 ± 1.5	6.1 ± 0.4
70.3	29.1 ± 1.4	6.6 ± 0.5
72.2	25.3 ± 1.6	5.4 ± 0.4
79.9	11.2 ± 0.9	2.7 ± 0.3

Table 2 (continued)

Lab. Angle degree	$(d\sigma/d\Omega)_{lab}$ (mb/sterad.)	
	4.8 Mev	6.9 Mev
4.9	2.18 ± 0.13	940 ± 190 x 10^{-3}
7.3	2.40 ± 0.15	840 ± 170
10.3	2.17 ± 0.13	700 ± 140
13.7	1.80 ± 0.11	600 ± 120
16.3	1.46 ± 0.09	530 ± 80
19.4	1.28 ± 0.08	470 ± 60
23.8	1.03 ± 0.04	405 ± 40
24.2	1.05 ± 0.04	412 ± 40
28.2	714 ± 28 x 10^{-3}	406 ± 38
31.5	501 ± 20	376 ± 31
34.8	337 ± 14	284 ± 22
39.2	204 ± 10	232 ± 14
44.7	129 ± 7	138 ± 8
49.7	93 ± 5	70 ± 5
54.7	54.4 ± 2.9	46.1 ± 3.4
60.0	37.5 ± 2.0	26.3 ± 2.1
63.4		
65.0	25.2 ± 1.6	18.4 ± 1.5
67.7		
70.3	15.9 ± 1.1	12.1 ± 1.1
72.2		
79.9	8.9 ± 0.7	5.8 ± 0.6

Fig. 19. Angular distributions for different deuteron groups produced from $C^{12}(p,d)C^{11}$ reaction.

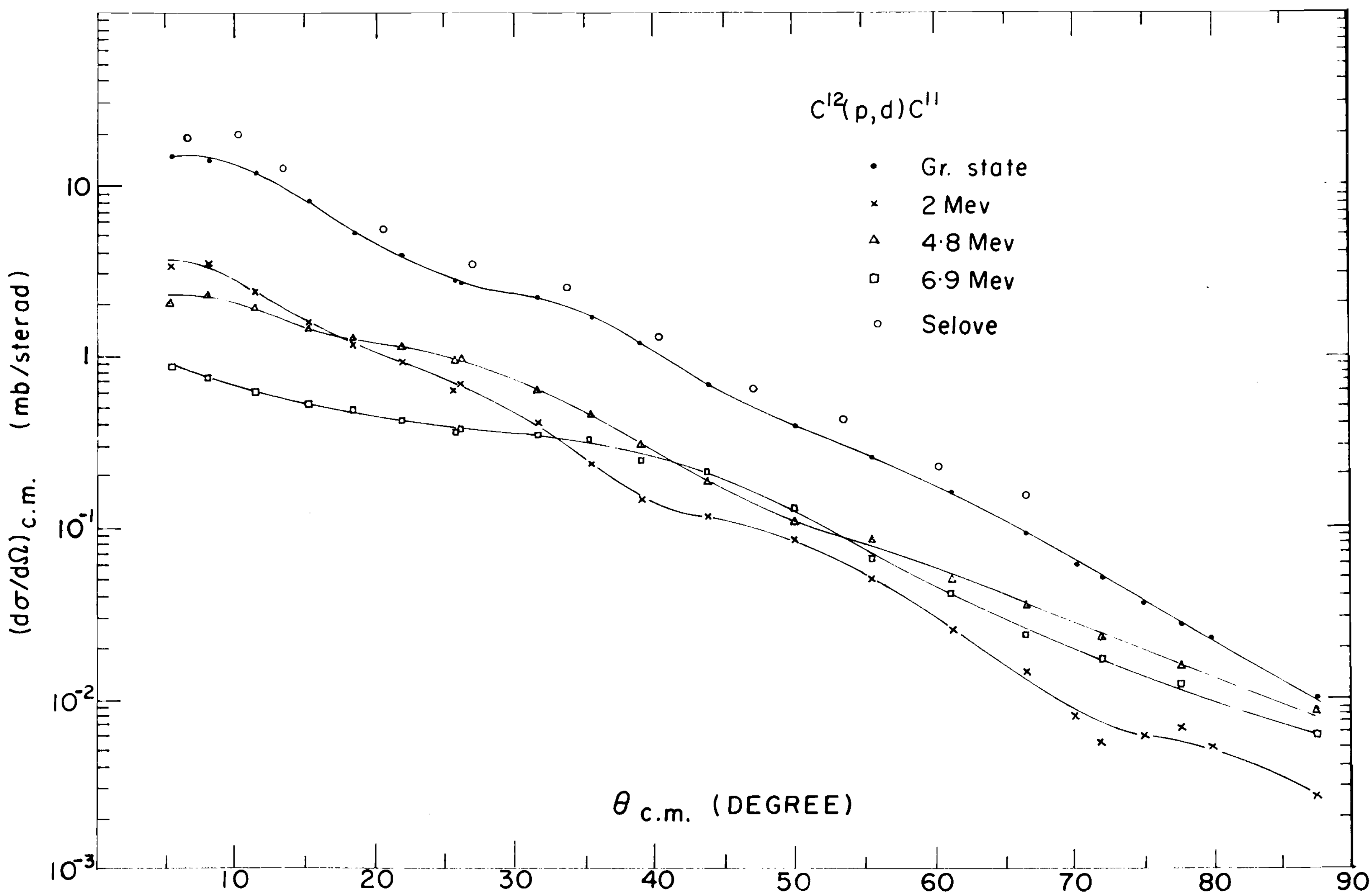
$C^{12}(p,d)C^{11}$
Gr. state
2 Mev
4·8 Mev
6·9 Mev
Selove
$(d\sigma/d\Omega)_{c.m.}$ (mb/sterad)
10
1
10^{-1}
10^{-2}
10^{-3}
$\theta_{c.m.}$ (DEGREE)
10
20
30
40
50
60
70
80
90

FIGURE 19

this be the case, then in the (p,d) reaction on C^{12}, $\ell=3$ will be necessary for the production of deuterons leading to the 6.9 Mev state in C^{11}. This then implies that the ground state of C^{12} will also have some configuration mixing in the 1f shell.

Austin et al (1962), in observing the γ-ray de-excitation of C^{11} produced in the $C^{12}(p,pn)C^{11}$ reaction at 120 - 150 Mev, obtained a considerable yield of 4.3 Mev, 6.3 Mev and 6.5 Mev states in C^{11} while the yield of the 6.9 Mev state was very weak. These results also indicated some configuration mixing of the 1f shell in the ground state of C^{12}. However, deuteron groups corresponding to 4.3 Mev, 6.3 Mev and 6.5 Mev states in C^{11} were not observed in the present work, and this seems to indicate that the reaction mechanism for (p,d) and (p,pn) reactions could be different.

Comparision of angular distributions of different deuteron groups from C^{12} and O^{16} is quite interesting. For deuteron groups corresponding to the pick-up of a $1p_{3/2}$ neutron (ground state of C^{11} and 6.2 Mev state in O^{15}), the angular distributions are very similar. Actually, for angles smaller than 40^{o}, they are identical to each other within experimental error. As for the deuteron groups corresponding to the pick-up of a $1p_{1/2}$ neutron (2 Mev state of C^{11}

and ground state of O^{15}), the angular distributions are different, but the diffraction patterns are quite similar. The diffraction peak observed in $O^{16}(p,d)O^{15}$ (ground state) was also observed in $C^{12}(p,d)C^{11}$ (2 Mev state). This strongly suggests the j-dependence of this type of reaction. The angular distribution of deuterons corresponding to the 6.9 Mev state of C^{11} is very different from the others and indicates that this may not be an ℓ=1 pick-up process.

C. $Li^7(p,d)Li^6$

The target used was natural lithium (92.6% Li^7 and 7.4% Li^6) rolled under kerosene to 69 mg/cm^2 thick. It was normally kept in kerosene, and was transferred to the scattering chamber just before the bombardment. Energy spectra of deuterons at 4.2^o, 23.8^o and 60.0^o are shown in Fig. 20 together with the energy level scheme of Li^6 (Ajzenberg-Selove 1959, Macfarlane 1960). The prominent peaks corresponded to the ground state (1+) and the excited states of 2.2 Mev (3+), 3.6 Mev (0+, T=1) and 5.4 Mev (2+, T=1) in Li^6.

The energy resolution obtained was about 1.3 Mev and the ground state and the 2.2 Mev state were distinctly separated. The 3.6 Mev state, however, could not be clearly resolved from the 2.2 Mev state and therefore gaussian graph

Fig. 20. Deuteron energy spectrums from lithium at 4.2°, 23.8° and 60.0° (lab. angles). The energy level scheme of Li^{6} is shown on top of the diagram. Dotted lines show the subtraction of continuum. The error bars shown are statistical uncertainties.

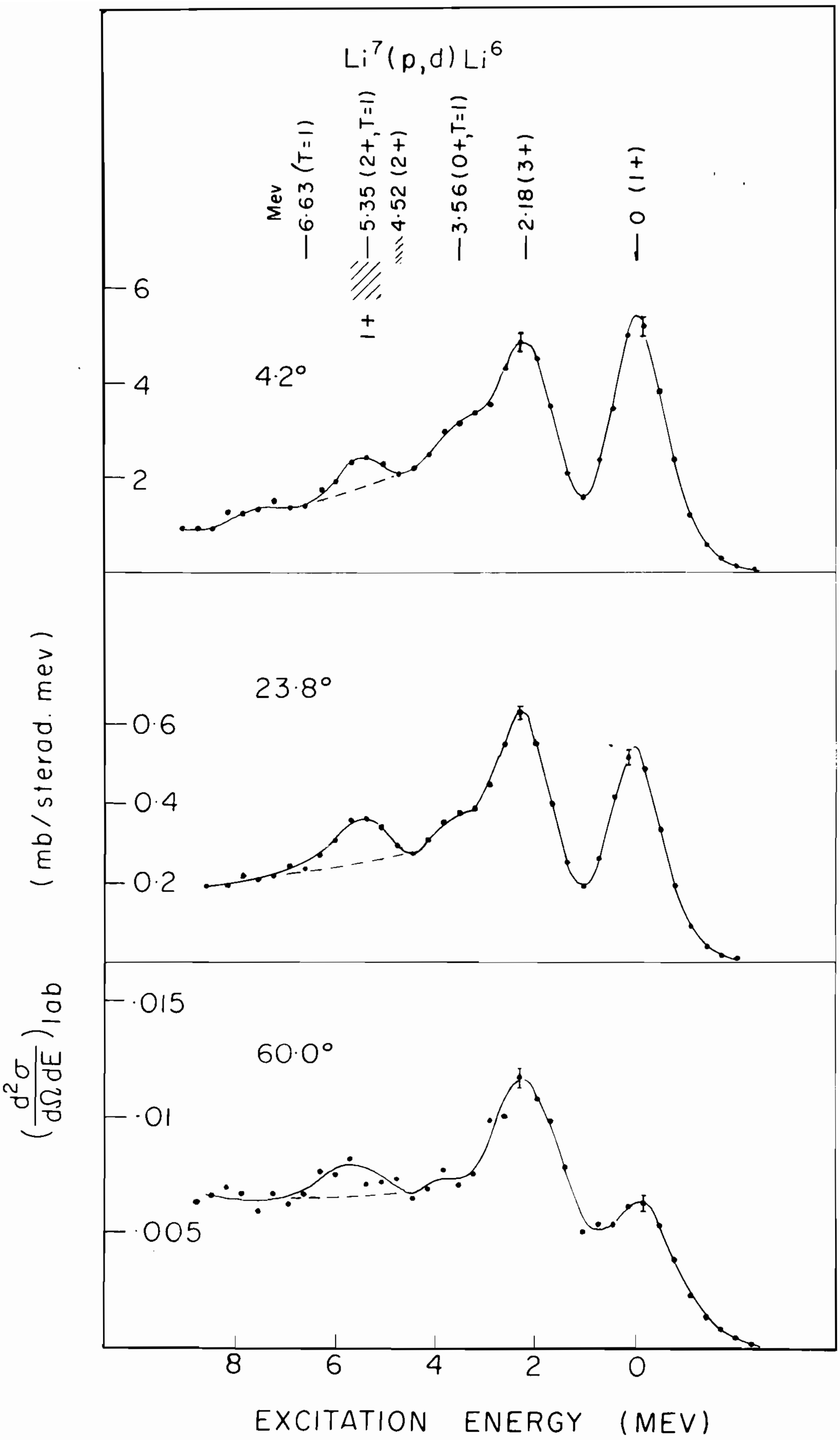

$Li^7(p,d)Li^6$
Mev
6·63 (T=1)
5·35 (2+, T=1)
4·52 (2+)
1+
3·56 (0+, T=1)
2·18 (3+)
0 (1+)
4·2°
23·8°
60·0°
6
4
2
0·6
0·4
0·2
·015
·01
·005
$\left(\frac{d^2\sigma}{d\Omega\, dE}\right)_{lab}$ (mb/sterad. mev)
8
6
4
2
0
EXCITATION ENERGY (MEV)

FIGURE 20

paper (Onno 1961) was used in the separation process. The uncertainty thus introduced depended on the statistics accumulated and should be less than 10% in the forward angular region. For scattering angles larger than 45°, the error introduced in the separation process became larger due to the increasing continuum under the peaks and the poorer statistics. The 5.4 Mev state was situated in the middle of a broad state (1+) centered at about an excitation energy of 5.5 Mev. In this work, it was impossible to separate the scattering from these two states, and therefore, only the upper and lower limits of area under the 5.4 Mev state were estimated. The upper limit was obtained by multiplying the peak height by the energy resolution which was obtained from the ground state peak. The lower limit was obtained by subtracting the continuum from the energy spectrum and then fitting a gaussion at the peak position as shown in Fig. 20.

For (p,d) reactions with the lithium target, the background introduced by the tritons and the nuclear reaction of deuterons in the NaI counter should be small and was neglected, and the uncertainties introduced were included in the relative uncertainty. Deuterons from the $Li^6(p,d)Li^5$ would not have any narrow peak since Li^5 was unstable to proton emmision, and since the contribution to background from this could not be estimated in the present work, they were included in the calculations. The uncertainty introduced (taken as 7%) was added to the absolute systematic uncertainty.

In an observation of the $Li^7(p,d)Li^6$ reaction using a particle separation system which exhibited the entire deuteron energy spectrum (Mark 1965), a broad peak of full width at half maximum of about 10 Mev was obtained at an excitation energy of about 23 Mev. This peak was also investigated with the better energy resolution of the system used in this work, but no prominent narrow peak was observed, and therefore no further study was carried out here.

The differential cross sections together with the relative uncertainties are tabulated in Table 3. The results were converted to the center of mass system and the angular distributions are shown in Figs. 21a and 21b.

Li^7 and Li^6 are stable isotopes and their level properties have been quite extensively investigated. In general, they can be quite satisfactorily described by an intermediate coupling scheme in shell model. Recently, Balashov et al (1965) used this intermediate coupling scheme and calculated the fractional parentage coefficients of the ground state of Li^7 with Li^6 as the residual nucleus, and found that all the levels up to and including the 5.5 Mev state in Li^6 could be parents of the ground state of Li^7. The reduced width thus deduced indicated that those of the 4.5 Mev

TABLE 3

Differential cross sections of the deuteron groups from the $Li^7\ (p,d)\ Li^6$ reaction.

Absolute systematic uncertainty $= {+8\% \atop -15\%}$

Lab. Angle degree	$(d\sigma/d\Omega)_{lab}$(mb/sterad.)	
	0 Mev	2.2 Mev
4.2	7.01 ± 0.42	6.52 ± 0.39
6.7	5.35 ± 0.32	5.03 ± 0.30
9.6	3.63 ± 0.22	3.41 ± 0.20
12.6	2.13 ± 0.13	1.94 ± 0.12
17.2	1.12 ± 0.07	1.13 ± 0.07
20.2	$908 \pm 55 \times 10^{-3}$	$953 \pm 57 \times 10^{-3}$
23.8	696 ± 23	825 ± 27
24.2	678 ± 23	818 ± 27
28.2	431 ± 15	639 ± 22
31.5	266 ± 9	453 ± 16
34.8	143 ± 6	269 ± 13
39.2	70.4 ± 3.5	115 ± 6
44.7	39.0 ± 2.1	70.3 ± 4.1
49.7	24.8 ± 1.5	43.6 ± 2.8
54.7	17.5 ± 1.1	27.2 ± 1.8
60.0	11.9 ± 0.9	19.4 ± 1.4
65.0	8.9 ± 0.7	13.9 ± 1.1
70.3	5.6 ± 0.6	10.5 ± 1.0

Table 3 (continued)

Lab. Angle degree	$(d\sigma/d\Omega)_{lab}$ (mb/sterad.)		
	3.6 Mev	5.4 Mev	
		cont. not subtracted	cont. subtracted
4.2	3.88 ± 0.29	3.06 (± 15%)	1.24 (± 20%)
6.7	3.52 ± 0.26	2.82	1.13
9.6	2.42 ± 0.19	2.04	821 x 10^{-3}
12.6	1.75 ± 0.14	1.24	632
17.2	905 ± 73 x 10^{-3}	787 x 10^{-3}	302
20.2	667 ± 56	627	260
23.8	477 ± 37	508	196
24.2	456 ± 37	481	186
28.2	368 ± 30	378	125
31.5	199 ± 17	243	72
34.8	146 ± 13	157	46
39.2	68 ± 7	93	24.2
44.7	27 ± 3	54	15.5
49.7	23.8 ± 2.8	36	8.9
54.7	21.2 ± 2.6	19.1	3.8
60.0	12.7 ± 1.7	12.3	2.1
65.0	7.1 ± 1.0	8.5	1.4
70.3	6.5 ± 0.9	6.5	1.0

Fig. 21. Angular distributions for different deuteron groups produced in $Li^7(p,d)Li^6$ reaction.

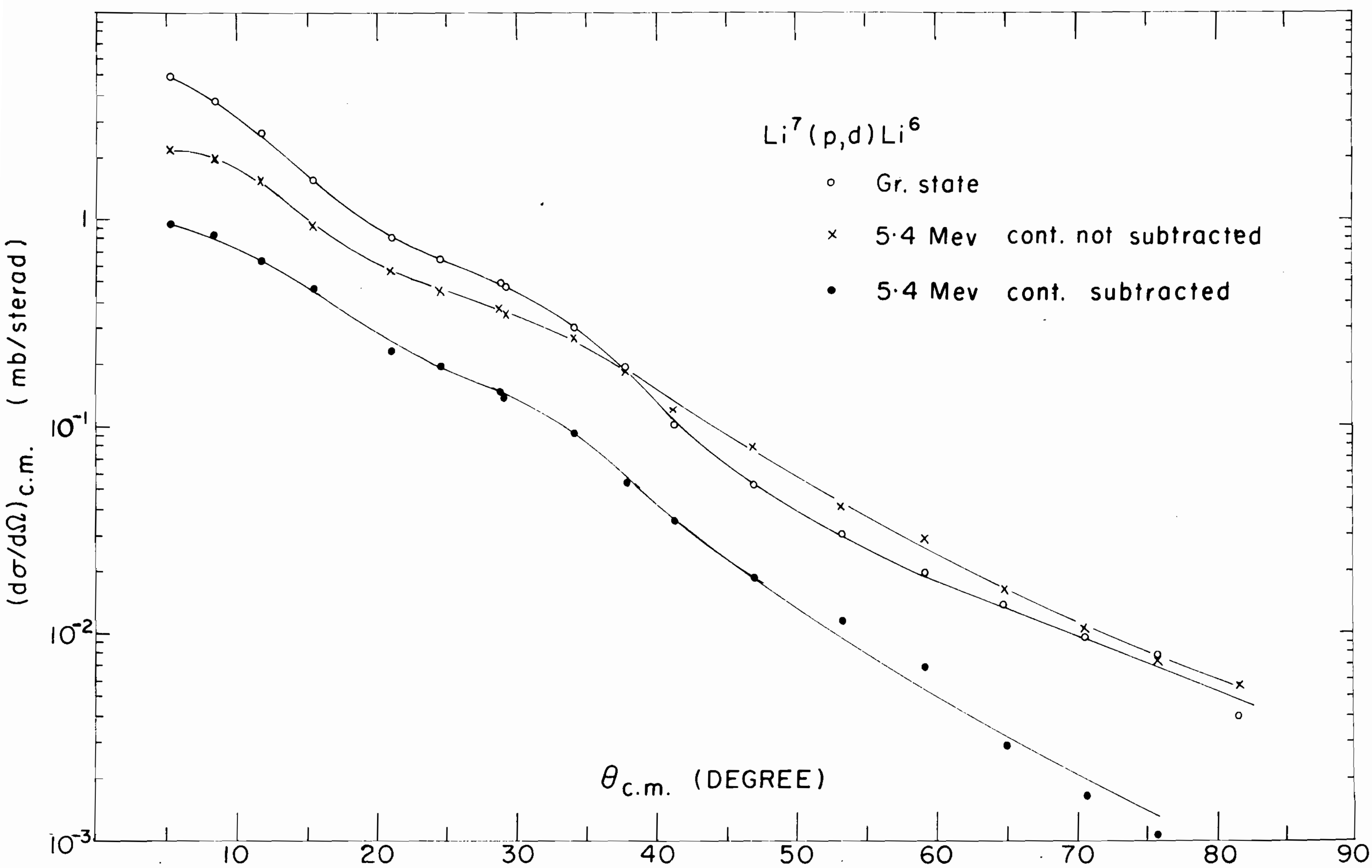
$Li^7(p,d)Li^6$
○ Gr. state
× 5·4 Mev cont. not subtracted
● 5·4 Mev cont. subtracted
$(d\sigma/d\Omega)_{c.m.}$ (mb/sterad)
1
10^{-1}
10^{-2}
10^{-3}
$\theta_{c.m.}$ (DEGREE)
10
20
30
40
50
60
70
80
90

FIGURE 21a

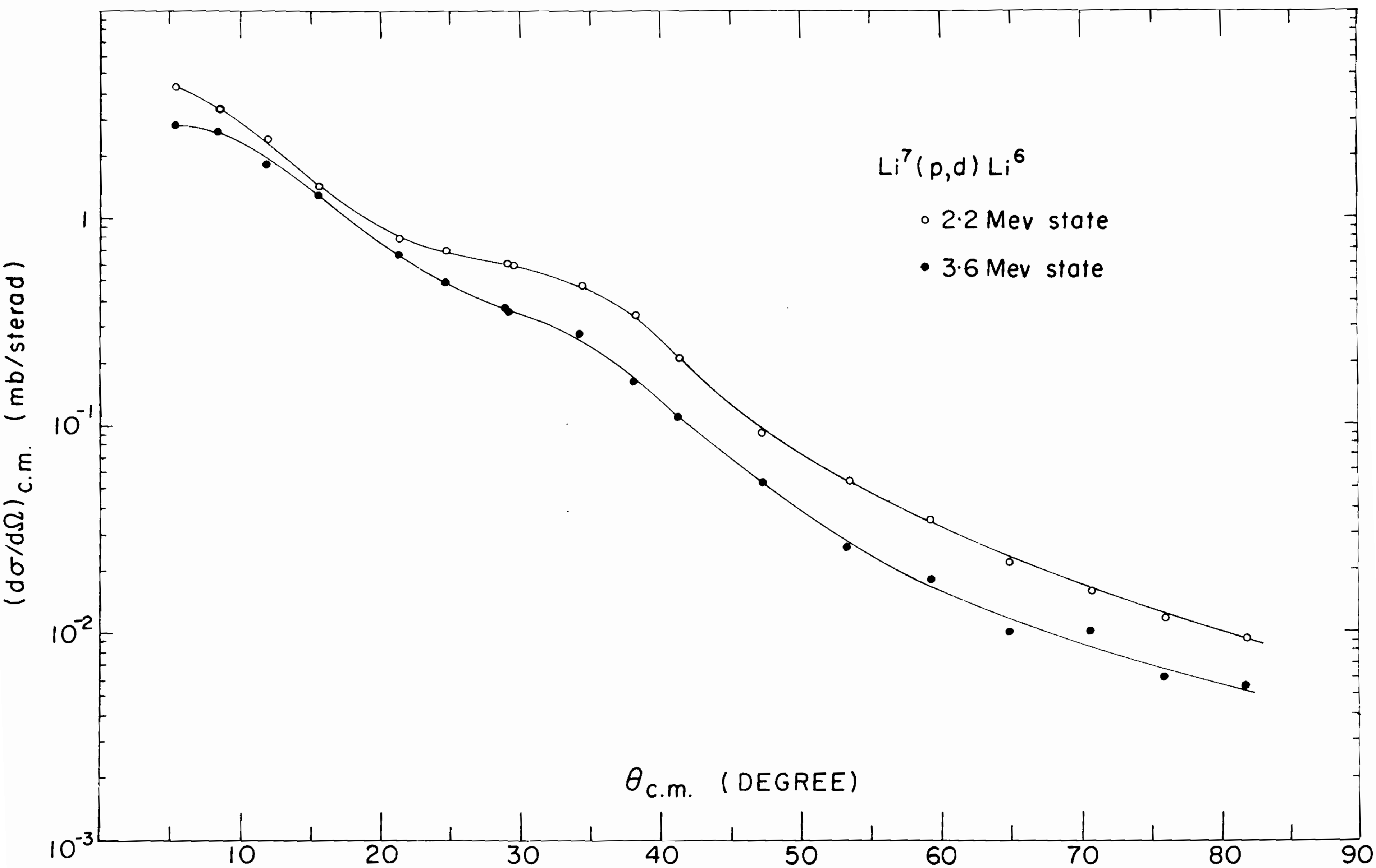

$Li^7(p,d)Li^6$
○ 2·2 Mev state
● 3·6 Mev state
$(d\sigma/d\Omega)_{c.m.}$ (mb/sterad)
$\theta_{c.m.}$ (DEGREE)
1
10^{-1}
10^{-2}
10^{-3}
10
20
30
40
50
60
70
80
90

FIGURE 21b

and 5.5 Mev states were much smaller, in agreement with the present results.

D. Summary and Conclusion

In the study of pick-up reactions such as (p,d) reaction in this energy range, one major difficulty is the separation of the desired particles from the background. The analysing magnet, with its capability of obtaining clean particle separation and good energy resolution, provides an excellent means for such studies. However, such an instrument for particles of this energy range will require large experimental space, and the energy resolution obtained is limited by the energy spread of the proton beam (about 1 Mev). In a concurrent project undertaken at this laboratory, dE/dx x E method was used (Mark 1965), and good particle separation over a wide range of energy was obtained. However, the energy resolution in that system was limited by the intrinsic energy resolution of the plastic scintillators used, and is not particularly suitable for the study of individual levels of the residual nuclei. In this work, a 14^{o}-deflecting magnet together with an analysing slit was designed to provide a momentum selection of the scattered particles. A counter telescope with solid state dE/dx-counters and a NaI E-counter was used to detect the desired particles. For the study of (p,d) reaction at 100 Mev, this system was found to be capable of excluding all the protons, though some feed-through of tritons may exist. The energy resolution obtained was 1.3 Mev and the major contributing factor was the energy spread of the proton beam used (about 1 Mev). With a mono-energetic proton beam and a thinner target, the present system should be able to give an energy resolution of 0.8 Mev or better, which should be close to the intrinsic resolution of NaI counter for deuterons of this energy range.

Angular distributions for the prominent deuteron peaks in $O^{16}(p,d)O^{15}$, $C^{12}(p,d)C^{11}$ and $Li^{7}(p,d)Li^{6}$ reactions were reported. Most of these angular distributions exhibit similar form and are believed to correspond to 1p shell neutron pick-up reactions. However, the angular distribution of deuterons corresponding to the 6.9 Mev state (perhaps the 4.8 Mev state as well) in C^{11} shows very different form and indicates that it is not a 1p shell neutron pick-up reaction. This will then imply that the ground state of C^{12} may have some configuration mixing in the upper shells. The fact that the angular distributions corresponding to the $1p_{1/2}$ shell neutron pick-up leading to the ground state of O^{15} and the first excited state of C^{11} exhibited diffraction peaks at about 75° seems to indicate that the (p,d) reactions at this energy depend on the total angular momentum transfer.

To extract further information from these results will require some form of distorted wave analysis and at present, there are still many uncertainties in such an approach. One of the reasons for these uncertainties is the lack of experimental data in this field, and it is hoped that the present results are a useful contribution to the data required.

BIBLIOGRAPHY

Amit D. and Karz A. Nuc. Phys. 58 (1964), 388.

Ajzenberg-Selove F. and Lauritsen T. Nuc. Phys. 11 (1959), 1.

Austin S.M., Salmon G.L., Clegg A.B., Foley K.J. and Newton D. Proc. Phys. Soc. 80 (1962), 383.

Bachelier D., Bernas M., Detraz C., Genin J., Haag J. and Radvanyi P. Proc. of Conference on Direct Interactions and Nuclear Reaction Mechanism at Padue (1962), 1141. Gordon and Breach Science Publisher, N.Y.

Bacholier D., Bernas M., Brissaud I., Detraz C., Ganguly N.K. and Radvanyi P. Phys. Let. 8 (1964), 56.

Balashow V.V., Boyarkina A.N. and Rotter I. Nuc. Phys. 59 (1965), 417.

Beltrametti E.G. and Tomasini G. Nuo. Cim. 18 (1960), 688.

Benioff P.A. Phys. Rev. 128 (1962), 740.

Bennett E.F. and Maxson D.R. Phys. Rev. 116 (1959), 131.

Burge E.J. and Smith D.A. Rev. Sc. Inst. 33 (1962), 1371.

Butler S.T. Nuclear Stripping Reactions (1957), John Wiley and Son, Inc., N.Y.

Cavanaugh P.E., Coleman C.F. Gard G.A., Ridley B.W. and Turner J.F. Nuc. Phys. 50 (1964), 61.

Chew G.F. and Goldberger M.L. Phys. Rev. 77 (1950), 470.

Clegg A.B., Foley K.J., Salmon G.L., and Segel R.E. Proc. Phys. Soc. 78 (1961), 681.

Cohen B.L., Mead J.B., Price R.E., Quisenberry K.S., and Martz C. Phys. Rev. 118 (1960), 499.

Cohen B.L., Fulmer R.H. and McCarthy A.L. Phys. Rev. 126 (1962), 698.

Cooper P. and Wilson R. Nuc. Phys. 15 (1960), 373.

Freeman R.M. Nuc. Phys. 37 (1962), 215.

Foley K.J., Salmon G.L. and Clegg A.B. Nuc. Phys. 31 (1962), 43.

Fulmer R.H. and Daehnick W.W. Phys. Rev. Let. 12 (1964), 455.

Glenddening N.K. Ann. Rev. of Nuclear Science 13 (1963), 191.

Goodman C.D. and Ball J.B. Phys. Rev. 118 (1960), 1062.

Greider K. Phys. Rev. 114 (1959), 786.

Hadley J. and York H. Phys. Rev. 80 (1950), 345.

Hess W.N. and Moyer B.J. Phys. Rev. 101 (1956), 337.

Igo G. and Eisberg R.M. Rev. Sc. Inst. 25 (1954), 450.

Jackson D.F. Nuc. Phys. 54 (1964), 561.

James A.N., Ferguson A.T.G. and Johnson C.M.P. Nuc. Phys. 25 (1961), 282.

Kavaloski C.D., Bassani G. and Hintz N.M. Phys. Rev. 132 (1963), 813.

Kurath D. Phys. Rev. 101 (1956), 216.

Lauritsen T. and Ajzenberg-Selove F. Nuclear Data Sheet (1962), National Research Council, Washington D.C.

Lee J.K.P. (1962) M.Sc. Thesis, McGill University (unpublished).

Lee L.L. Jr. and Schiffer J.P. Phys. Rev. 136 (1964), B405.

Lee L.L. Jr., Marinov A., Mayer-Boricke C., Schiffer J.P., Bassel R.H., Drisko R.M. and Satchler G.R. Phys. Rev. Let. 14 (1965), 261.

Legg J.C. Phys. Rev. 129 (1963), 272.

Macfarlane M.H. and French J.B. Rev. Mod. Phys. 32 (1960), 567.

Macfarland M.H. Proc. of Conference on Direct Interactions and Nuclear Reaction Mechanisms at Padue (1962), 3. Gordon and Breach Science Publisher, N.Y.

Mark S.K. (1965) Ph.D. Thesis, McGill University (unpublished).

Matsuda K., Proc. of Conference on Direct Interactions and Nuclear Reaction Mechanisms at Padue (1962), 499. Gordon and Breach Science Publisher, N.Y.

Onno P., Rev. Sc. Inst. 32 (1961), 1253.

Penner S. Rev. Sc. Inst. 32 (1961), 150.

Radvanyi P., Genin J. and Detraz C. Phys. Rev. 125 (1962), 295.

Rowe D.J., Clegg A.B., Salmon G.L. and Fisher P.S. Proc. Phys. Soc. 80 (1962), 1205.

Sherr R., Rost E. and Rickey M.E. Phys. Rev. Let. 12 (1964), 420.

Selove W. Phys. Rev. 101 (1956), 231.

Selove W. and Teem J.M. Phys. Rev. 112 (1958), 1658.

Tanner N.W. and Earle E.D. Phys. Rev. Let. 13 (1964), 410.

Tyren H., Hillman P. and Maris T.A.J. Nuc. Phys. 7 (1958), 10.

Wilkinson D.H. Proc. of the International Conference on Nuclear Structure at Kingston (1960), 20. University of Toronto Press, Toronto.